TAMPEREEN TEKNILLINEN YLIOPISTO
TAMPERE UNIVERSITY OF TECHNOLOGY

ILKKA HOKAJÄRVI

ELECTRODE CONTACT IMPEDANCE AND BIOPOTENTIAL SIGNAL QUALITY

Master of Science thesis

Examiner: Professor Jari Hyttinen
Examiner and topic approved in
the Faculty of Computing and
Electrical Engineering Council
meeting on December 7, 2011

ABSTRACT

TAMPERE UNIVERSITY OF TECHNOLOGY
Master's Degree Programme in Electrical Engineering
ILKKA HOKAJÄRVI: Electrode Contact Impedance and Biopotential Signal Quality
Master of Science Thesis, 66 pages, 3 Appendix pages
September 2012
Major: Biomedical Engineering
Examiner: Professor Jari Hyttinen
Keywords: artifact, biopotential, electrode, ECG, EEG, impedance, noise

Electroencephalography (EEG) is the recording of potential fluctuations originating from electrical activity of brain. It is used in diagnosis of neurological disorders, monitoring the depth of anaesthesia and evaluation of sleep. A possible application is long-term continous monitoring of intensive care unit (ICU) patients, with the aim to detect epileptic seizure activity. Currently this is not practised due to poor usability of the available equipment. This thesis is part of a project which aims to develop a novel solution which solves the usability problem. Adding to that, the solution contains an algorithm for automatic online epileptic seizure detection, which enables immediate treatment of patients once epileptic seizures occur. This leads to an increased patient outcome at ICUs.

An imporant factor contributing to poor usability of current EEG equipment is the electrode contact. To ensure good signal quality, skin under the electrodes needs to be prepared by abrasion for example. This is time-consuming especially when multiple electrodes are used. Adding to that, skin preparation damages skin which is undesired especially in long-term applications, as the the presence of electrode and electrolytic gel causes irritation and possibly an infection risk. The quality of the electrode contact is quantified by its electrical impedance.

In this thesis the relationship of electrode contact impedance to total electrode contact noise and motion artifact magnitude are studied. These both are factors contributing to biopotential signal quality. Sintered silver-silverchloride electrodes are used in the work. Contact impedance is defined as the magnitude of the impedance vector at $20\,\mathrm{Hz}$. Contact noise is studied by measuring impedance-noise data pairs (n=122) at two body sites of volunteer subjects using two different electrode gels. A univariate analysis of variance is implemented on the data pairs. Motion artifact magnitude is studied with impedance-artifact magnitude data pairs (n=33) while producing a horizontal motion to the electrode. The behavior of the seizure detection algorithm is also studied by adding different amounts of noise to EEG signals, and assessing how its behavior changes.

The results show that electrode contact impedance can be used as a rough predictor of total contact noise. With contact impedance in the range of $20\,\mathrm{k}\Omega$ or less, the contact noise is expected to settle at RMS values less than $5\,\mu\mathrm{V}$ at a $30\,\mathrm{Hz}$ bandwidth. It was also found the that the type of electrolytic gel can have a significant effect on total contact noise. Motion artifact magnitude was found to decrease with decreasing contact impedance. With larger contact impedance values, the variations of motion artifact magnitudes were larger. The behavior of the seizure detection algorithm was found to change significantly with a small amount of noise added to EEG signals. By comparing that amount of noise to the measured contact noise data, it can be seen that it is well within the measured values.

TIIVISTELMÄ

TAMPEREEN TEKNILLINEN YLIOPISTO
Sähkötekniikan koulutusohjelma
ILKKA HOKAJÄRVI: Elektrodikontaktin impedanssi ja biopotentiaalisignaalin laatu
Diplomityö, 66 sivua, 3 liitesivua
Syyskuu 2012
Pääaine: Lääketieteellinen tekniikka
Tarkastaja: professori Jari Hyttinen
Avainsanat: artefakta, biopotentiaali, elektrodi, EEG, EKG, impedanssi, kohina

Elektroenkefalografiassa (EEG) rekisteröidään aivosähkötoiminnasta syntyviä potentiaalivaihteluita. EEG:tä käytetään neurologisten sairauksien diagnosoinnissa, anestesian syvyyden mittauksessa sekä unen vaiheiden tutkimisessa. Tehohoitopotilaiden jatkuvatoiminen ja pitkäaikainen EEG-rekisteröinti epileptisten kohtausten havaitsemiseksi on mahdollinen uusi sovellusala. Toistaiseksi tätä sovellusalaa rajoittaa saatavilla olevien laitteiden huono käytettävyys. Tämä diplomityö on osa projektia, jossa pyritään kehittämään tämän käytettävyysongelman ratkaiseva tuote. Tuotteeseen kuuluu myös algoritmi, joka havaitsee epileptiset kohtaukset ajantasaisesti. Tämän seurauksena potilaiden hoito voidaan aloittaa heti kohtauksen alettua, joka johtaa parempaan hoidon vasteeseen.

Elektrodikontaktilla on merkittävä vaikutus EEG-laitteiden käytettävyyteen. Hyvälaatuisen signaalin saamiseksi ihoa raaputetaan elektrodien sijaintipaikoilta. Eritysesti monia elektrodeja hyödyntävissä sovelluksissa tämä vie aikaa. Ihon raaputus myös vaurioittaa ihoa, joten se tulisi minimoida. Erityisen tärkeää tämä on pitkäaikaisissa sovelluksissa, sillä elektrodi sekä elektrolyyttigeeli aiheuttavat ärsytystä sekä mahdollisesti jopa infektioriskin vaurioituneella iholla. Elektrodikontaktin laatu määritellään sen impedanssin perusteella.

Tässä työssä tutkitaan elektrodikontakin impedanssin suhdetta elektrodikontaktissa syntyvään kohinaan sekä elektrodin liikkeestä aiheutuvien artefaktojen suuruuteen, jotka molemmat ovat biopotentiaalisignaalin laatuun vaikuttavia tekijöitä. Työssä käytetään sintrattuja hopea-hopeakloridielektrodeja. Kontakti-impedanssi mitataan 20 hertsin taajuudella. Elektrodikontaktin kohinaa tutkitaan muodostamalla impedanssi-kohina datapisteitä (n=122) koehenkilöistä mittaamalla kahta elektrodien sijaintia ja kahta elektrolyyttigeeliä käyttäen. Datapisteille tehdään yksisuuntainen varianssianalyysi. Liikeartefaktojen suuruutta tutkitaan muodostamalla impedanssi-artefakta datapisteitä (n=33) kun elektrodia liikutetaan vaakasuuntaisesti. Epileptisten kohtausten havaitsemiseksi kehitetyn algoritmin toimintaa tutkitaan lisäämällä EEG-signaaleihin eri määriä kohinaa ja suorittamalla algoritmi kohinaisille signaaleille.

Työn tulokset osoittavat, että elektrodikontakin kohinaa voidaan ennustaa kontakti-impedanssin perusteella. Kohinan neliöllinen keskiarvo pysyy pienempänä kuin $5\,\mu\mathrm{V}$ $30\,\mathrm{Hz}$ kaistanleveydellä impedanssin ollessa $20\,\mathrm{k}\Omega$ tai sen alle. Elektrolyyttigeelin tyypillä on merkittävä vaikutus kohinan suuruteen. Liikeartefaktojan havaittiin olevan sitä pienempiä, mitä pienempi kontakti-impedanssi on. Impedanssiarvon kasvaessa liikeartefaktojen suuruuksien hajonta kasvoi. Suuruudeltaan pienen kohinasignaalin lisääminen EEG-signaaliin vaikutti alogritmin toimintaan merkittävästi. Verrattaessa lisättyä kohinaa mitattuihin kohinadatapisteisiin havaittiin lisätyn kohinan olevan mittaustulosten alueella.

PREFACE

The topic of this thesis was provided by GE Healthcare Finland Oy. During the work I was a member of the Technology Research team. First of all I would like to express my gratitude to both of my instructors, Kimmo Uutela and Juha Virtanen, for their guidance and advice during the process. I am also grateful to Antti Tanner, Emma Ikonen and Mika Särkelä for their cooperation. Special thanks go to everyone who volunteered as test subjects in the experiments. I would also like to thank Professor Jari Hyttinen for his help on behalf of Tampere University of Technology.

During the process I have learned a lot, be it from technical, clinical or whatever other issues. I have been deeply inspired by seeing skilled and motivated professionals at work every day. All my colleagues deserve thanks for providing such a pleasant working environment.

Finally, I would like to thank my family and friends for their support during this process and the whole length of my studies.

Lahti, August, 2012

Ilkka Hokajärvi

CONTENTS

SYMBOLS AND ABBREVIATIONS

Symbols

a	activity
A	area
A^-	chemical symbol of anion
Ag	chemical symbol of silver
B	magnetic flux density
c	concentration
C	capacitance
C^+	chemical symbol of cation
Cl	chemical symbol of chlorine
E	electric potential
e^-	chemical symbol of electron
f	frequency
F	Faraday's constant, $F = 9.648\,533\,652\,1 \cdot 10^4\,\mathrm{C\,mol^{-1}}$
G	voltage gain
I, i	electric current
k_b	Boltzmann's constant, $k_b = 1.380\,648\,813 \cdot 10^{-23}\,\mathrm{J\,K^{-1}}$
n	valence number
p	pressure
R	resistance
R_m	molar gas constant, $R_m = 8.314\,462\,175\,\mathrm{J\,K^{-1}\,mol^{-1}}$
T	absolute temperature
ΔT	time interval
u	mobility
V, v	voltage
Z	impedance

Abbreviations

AC	alternating current
Ag-AgCl	silver-silverchloride
CMRR	common-mode rejection ratio
DC	direct current
DFT	discrete Fourier transform
DRL	driven right leg
ECG	electrocardiogram, electrocardiography
EEG	electroencephalogram, electroencephalography
EMG	electromyogram
EOG	electro-oculogram
IA	instrumentation amplifier
ICU	intensive care unit
PSD	power spectral density
RF	radio frequency
RMS	root mean square
SATP	standard atmospheric temperature and pressure

1. INTRODUCTION

Electrical activity of biological systems is most often studied by measuring potential fluctuations, that is biopotential signals. In the field of medicine, certain biopotential signals are highly significant considering diagnosis and patient monitoring. Electroencephalography (EEG) is the recording of potential fluctuations originating from electrical activity of brain. The resulting signal is termed electroencephalogram. EEG is used in diagnosis of neurological disorders, monitoring the depth of anaesthesia, and evaluation of sleep. Electrocardiography (ECG) is the procedure to record potential fluctuations caused by electrical activity of heart, and it is routinely used in diagnosis of abnormal heart rhytms. Both EEG and ECG are based on the same principles. However, the electrical signals originating from brain are an order of magnitude smaller which results in a more restrictive nature of EEG compared to ECG. The focus of this thesis will be on EEG, but the concepts are applicable to ECG as well as recording of other biopotential signals.

EEG is most often studied by recording spontaneous electrical activity of brain. Spontaneous activity can produce voltage signals with a magnitude of a hundred microvolts when measured on the scalp, and a frequency bandwidth from under 1 to 50 Hz. In addition to small amplitudes, some other characteristics specific for EEG and other biopotential signals are high source impedances and relatively strong undesired signals obscuring the signal of interest. These characteristics set particular requirements for the used measurement instruments. Consequently, specially designed amplifiers, so called biopotential amplifiers are used.

Biopotential signals are results of ionic currents. In electrical instruments the signals are based on movement of electrons. Biopotential electrodes are transducers that convert ionic currents to electric currents at the interface between biological systems and measurement instruments. They come in a variety of forms and materials. However, the most commonly used type is a passive silver-silverchloride (Ag-AgCl) surface electrode. Other commonly used electrode materials include platinum, gold and stainless steel. Ag-AgCl is preferred to other materials in many cases due to its four favorable characteristics: a low and stable half-cell potential, low level of intrinsic noise, a relative non-polarizability, and small metal-electrolyte interface impedance [1].

As mentioned earlier, one characteristic specific for EEG is the presence of relatively strong undesired signals. These undesired signals include noise, artifacts and interference, and they are superimposed on the signal of interest. In order for EEG to have a clinical

value, the signal needs to be of a good quality which means a good elimination of all the undesired signals. Biopotential electrodes have a significant impact on biopotential signal quality, as the major part of all the undesired signals are related to them [2].

The quality of electrode-skin contact is critical to successful recording of biopotential signals. The contact quality can be quantified by electrode contact impedance, which is the property of the electrode-skin contact to oppose time-varying electric current. The skin under electrodes is usually prepared by abrasion in order to reduce electrode contact impedances. However, this can cause irritation and even pain, and is therefore undesired. Moreover, it is time-consuming especially in applications such as EEG where multiple electrodes are used.

This thesis aims to find out how accurately biopotential signal quality can be predicted with electrode contact impedance. Previously, Huigen et al. have found a relationship to exist between electrode contact impedance and noise [2]. Adding to that, Tam and Webster, and de Talhouet and Webster have found a relationship between electrode contact impedance and motion artifact magnitude [3,4]. Both contact noise and motion artifacts are factors contributing to biopotential signal quality.

The work in this thesis also includes studying the operation of an algorithm for epileptic seizure detection [5], with the aim to quantify a level of signal quality which significantly affects the algorithm operation. This thesis will also provide implications of the results to the design of biopotential amplifiers.

1.1 Context of the thesis

This thesis is a part of a project aiming to develop a novel solution for continuous and automatic detection of epileptic seizure activity. It is intended to be used for sedated or unconscious patients in intensive care units (ICU). Currently, continuous long-term EEG monitoring is not used routinely at ICUs. Instead epileptic seizures are detected by neurologists offline, meaning that they have already occurred when the seizures are detected. If seizures are automatically detected online, the treatment can be started immediately. This leads to an increased prevention of irreversible brain damage and reduced mortality of ICU patients. The main reason EEG is not monitored continuously at ICUs is the poor usability of the currently available equipment.

The aimed solution of this project includes three main components: an easy-to-use EEG headset with integrated electrodes, an algorithm for automatic detection of epileptic seizures, and the electronics which operate the whole system. The headset is critical considering usability. Several EEG headsets are available on the market, but their applicability to continous long-term EEG monitoring is limited. Factors contributing to this include uncomfortability to be worn for an extended time period, the need to attach all electrodes one by one, poor long-term reliability of electrode contact, and the lack of possibility to fix detached electrodes. These issues are discussed in detail in previous work

by Ikonen [6]. That work also describes creation of various headset prototypes. An illustration of the most recent headset prototype is presented in Fig. 1.1. The headset will be implemented with passive Ag-AgCl surface electrodes.

Clinical use of the headset provides numerous challenges to its design. Considering the work in this thesis the following challenges are of a great importance. First of all, the headset should be easily and quickly installable. The required amount of skin preparation prior to monitoring is a critical factor considering the easiness of the headset installation. Additionally, irritation and damage to skin should be minimal to minimize the caused pain and time of recovery after the monitoring. Moreover, the presence of electrodes and electrolytic gel at a damaged skin site for multiple days creates an infection risk which naturally should be minimized. Furthermore, the quality of recorded EEG signal is affected by the electrode contact impedances. Thus, the contact impedances should still be as low as possible which means that skin preparation is needed.

The seizure detection algorithm is described in previous work by Tanner [5]. The algorithm also utilizes a motion artifact rejection algorithm by Savelainen [7]. As electrode contact impedances and biopotential signal quality are related, it is of a great interest to study how the algorithm behaves with noisy signals. It would be useful if we can determine a limit to the signal quality at which the algorithm no longer behaves correctly.

The third component of the solution, the electronics, will be designed in the future. It will consist of a front-end module connected to a back-end patient monitor. Considering this thesis, the biopotential amplifier of the front-end electronics is important, as the interaction of the electrode contact and biopotential amplifier is critical to signal quality. In summary, the work in this thesis contains subject matters related to all of the three components of the aimed solution.

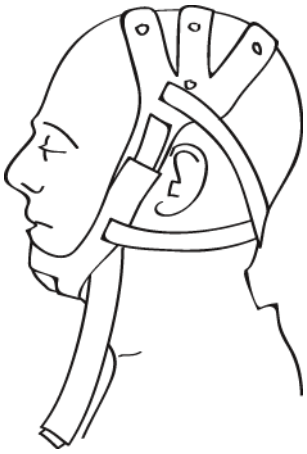

Figure 1.1. *Illustration of the EEG headset by Emma Ikonen.*

2. THEORETICAL BACKGROUND

2.1 Introduction to EEG

In 1924, Hans Berger recorded the first human EEG. He noticed that the electrical activity of brain changes according to the general status of a patient. He also noted that pathologic conditions could have an effect on the electrical activity of brain. [8] This section will provide a brief introduction to EEG and present an example of an epileptiform EEG signal.

2.1.1 EEG recording system

Ionic currents in neurons of the brain cause potential fluctuations on the scalp. The potential fluctuations are measured with biopotential electrodes. The so called 10-20 system is used to standardize the electrode positions for normal spontaneous activity EEG recordings [9]. The system consists of 21 electrodes in total. However, in some applications a reduced amount of electrodes is sufficient.

An EEG recording system contains the electrodes, an amplifier and a recorder at minimum. Two electrodes connected to an amplifier are referred to as a channel. A montage consists of multiple channels. The montage can be of a referential or of a bipolar type. In referential montage the potential of each electrode is compared to that of a single reference electrode. In bipolar montage the potential differences between different electrode pairs are measured. EEG signal is the conditioned output voltage of one EEG channel. Typically conditioning includes amplification and filtering. In modern EEG recording systems the signals are sampled and converted to a digital representation prior to storage in memory of a computer and possible further data processing and analysis.

2.1.2 EEG signal

When measured on the scalp, the amplitude of an EEG is typically $100\,\mu V$. Most of the time the signal is irregular with no patterns. At times, however, distinct patterns can be observed. The patterns can be inherent to specific abnormalities such as epileptic seizures, or they can belong to the wave groups of normal persons [10]. The wave groups are presented in Table 2.1.

At frequencies below $3.5\,Hz$ the waves are classified as Delta waves, and they are typically present during deep sleep. Theta waves between at 4–$7\,Hz$ are mostly present on

Table 2.1. *EEG waves and the respective frequency bands. [10]*

Wave	Δf [Hz]
Delta (δ)	0–3.5
Theta (Θ)	4–7
Alpha (α)	8–13
Beta (β)	14–30

parietal and frontal regions in children, and in some adults they occur during emotional stress. Waves between 8 and 13 Hz are Alpha waves which are present in normal persons in an awake resting state. Frequencies from 14 to 30 Hz are classified as Beta waves, and they are affected by mental activity of a person. Additionally, higher frequencies can also be present in EEG signal. At around 40 Hz so-called gamma waves exist. Moreover, during epileptic seizures local bursts at frequencies over 200 Hz can be observed. [10,11]

2.1.3 Epileptiform EEG

Types of epileptic seizures, their intensity, duration, and frequency tend to vary significantly between different patients. However, repetition of a similar seizure pattern for a single patient is common. Epileptic seizures occur not only on patients with diagnosed epilepsy, but also on other individuals. ICU patients are a typical example of a group of people where epileptic seizures can occur.

Figure 2.1 presents an example of an EEG tracing of a pattern of epileptic seizure evolution. Initially the frequency of the signal increases. After that the signal amplitude increases as well. At the end of the presented signal, post-ictal suppression occurs. However, this is only an example of a very clear seizure pattern, and most seizures do not follow this pattern or are much more unclear.

2.2 Biopotential electrodes

A biopotential electrode is a transducer which converts ionic currents to electric currents or vice versa. Although biopotential electrodes might look simple, their operating principles are quite complex. This section will provide insight into the operation of passive biopotential electrodes, and Ag-AgCl electrodes in particular.

2.2.1 Electrochemical basis

A biopotential electrode consists of two layers: a piece of metal is coated with an ionic compound of that specific metal with an anion. In the case of an Ag-AgCl electrode, $AgCl$ compound is deposited on top of plain Ag metal base. In order to enable charge transfer between biological tissue and a biopotential electrode, an electrolyte is needed between them. An electrolyte is any substance with free ions, thus causing it to be electrically

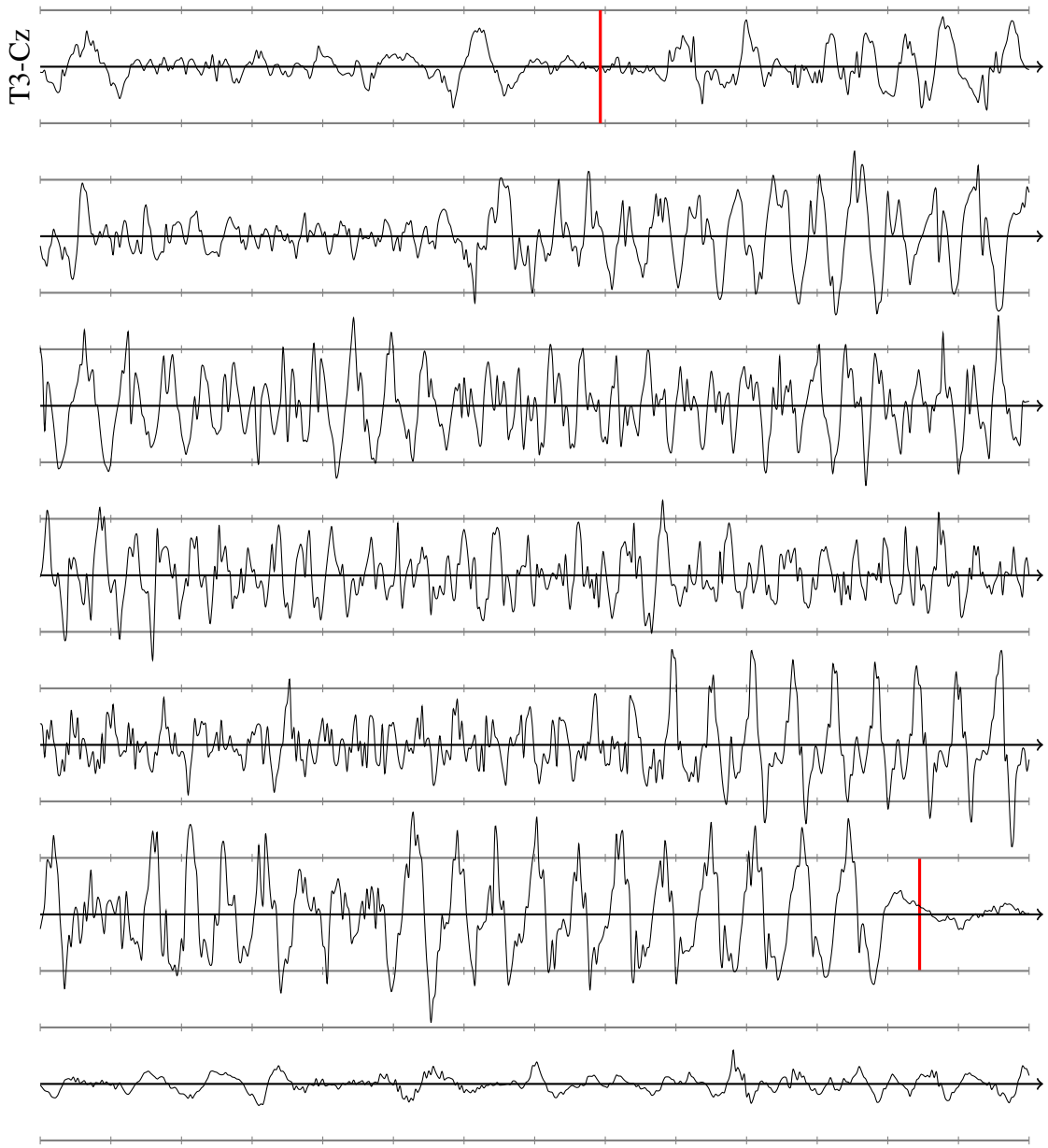

Figure 2.1. *EEG tracing during an example epileptic seizure evolution. The red lines indicate start and end points of the seizure. The tick marks on the horizontal axes indicate one second intervals, and the gray lines on top and bottom of the baseline level indicate* $\pm 50\,\mu V$ *amplitude levels.*

conductive. The electrolyte usually comes in form of an electrolytic gel which contains Cl^- anions.

Transfer of charge over the metal-electrolyte interface occurs due to chemical oxidation-reduction reactions. Generally the reactions can be presented by the following equations

$$C \rightleftharpoons C^{n+} + ne^- \tag{2.1}$$

$$A^{n-} \rightleftharpoons A + ne^- \tag{2.2}$$

where C^+ is a metallic cation, A^- is an electrolytic anion, n is the valence of ions and e^- denotes an electron [12]. Equation 2.1 describes the oxidation-reduction of metallic atoms and equation 2.2 describes that of electrolytic ions. In an optimal case these reactions are reversible, meaning that they occur equally easily in both directions.

In the case of an Ag-AgCl electrode, the reversible oxidation-reduction reactions occurring at the metal-electrolyte interface are

$$Ag \rightleftharpoons Ag^+ + e^- \tag{2.3}$$

$$Ag^+ + Cl^- \rightleftharpoons AgCl \tag{2.4}$$

When metal is positively charged compared to electrolyte, it gains chloride ions that are deposited on it. When it is negatively charged compared to the electrolyte, Ag-AgCl is reduced to Ag^+ and Cl^- ions. [12]

2.2.2 Double layer and half-cell potential

When a metal is brought in contact with an electrolyte, the ion concentration near the interface will be specifically distributed. Metallic ions tend to enter the electrolyte and ions from the electrolyte tend to combine with metal. This kind of charge distribution where ions with one sign of charge are bound to metal and oppositely charged ions are bound to electrolyte is known as the electrical double layer. [13]

The charge distribution causes a potential at the metal-electrolyte interface. This potential is known as the half-cell potential E_0. For different electrode materials, the characteristic E_0 values are different. The characteristic E_0 values are defined with respect to a hydrogen electrode because it is not possible to measure a potential of a single electrode with respect to a solution. Adding to that, it would be very impractical to tabulate all different potentials with respect to different electrolytes. Moreover, the hydrogen electrode can be easily reproduced in a laboratory. [13] Some examples of different E_0 values of different electrode materials and electrochemical reactions are presented in Table 2.2. Compared to other materials, Ag-AgCl has a low value of E_0.

Table 2.2. *Half-cell potentials of different electrode materials and electrochemical reactions. [12]*

Material	Reaction	E_0 [V]
aluminium	$Al \rightarrow Al^{3+} + 3e^-$	-1.706
hydrogen	$H_2 \rightarrow 2H^+ + 2e^-$	0.000 (by definition)
silver	$Ag + Cl^- \rightarrow AgCl + e^-$	+0.223
gold	$Au \rightarrow Au^+ + e^-$	+1.680

2.2.3 Polarization

The tabulated half-cell potentials of different electrode materials are measured in standard atmospheric temperature and pressure (SATP) conditions ($T = 25\,°\text{C}$, $p = 101\,325\,\text{Pa}$). In reality, however, the half-cell potential changes with varying temperature and ion activities. The half-cell potantial E_{hc} behaves according to the Nernst equation

$$E_{hc} = E_0 + \frac{R_m T}{nF} \ln\left(a_{M+}\right) \tag{2.5}$$

where E_0 is the half-cell potential in SATP conditions, R_m is the molar gas constant, T is the absolute temperature, n is the valence of the involved ion, F is the Faraday constant and a_{M+} is the activity of the metallic ion on the electrolyte [13]. Adding to the electrode material, temperature and electrolytic ion concentration, also movement of electrode causes changes in E_{hc}. The half-cell potential of Ag-AgCl electrodes is quite stable compared to other electrode materials [1].

Current flow through the electrode also causes variations in E_{hc}. This is due to polarization of the electrode. When current is flowing, the metal-electrolyte interface is out of equilibrium. The term overpotential is used to define the difference of the non-equilibrium and SATP half-cell potentials. There are three components contributing to overpotential. The first component is ohmic overpotential. The resistivity of an electrolyte is a function of current flowing through it. According to Ohm's law, a voltage drop occurs which is a function of resistivity and passing current. Should the electrolytic ion concentration be low, the relationship of resistivity and current can be nonlinear. The second component causing overvoltage is concentration overpotential. In a state of equilibrium, the oxidation-reduction reactions of equations 2.1 and 2.2 would occur at an equal velocity. However, in a non-equilibrium state the velocities of the reactions are inequal, thus causing a change in the electrolytic ion concentration. The last component, activation overpotential, is caused by the differences of activation energies of chemical reactions of equations 2.1 and 2.2. In a state of equilibrium the activation energies would be equal. Due to dominance of either the oxidation or the reduction reaction in a non-equilibrium state, however, the activation energies are inequal. [12]

When an electrode is described as perfectly polarizable, no net transfer of charge will travel through the metal-electrolyte interface. This results in a perfectly polarizable electrode to have the same characteristics as an ideal capacitor. On the opposite, when charge carriers are able to cross the metal-electrolyte interface unhindered, the electrode is perfectly non-polarizable. A perfectly non-polarizable electrode would have a fully stable half-cell potential. The electrodes of the real world are neither perfectly polarizable nor perfectly non-polarizable. In reality, the properties of electrodes fall somewhere in between these two extremes. [13] The Ag-AgCl electrode is the closest to a non-polarizable electrode which means that is has a low value of charge transfer resistance [1].

2.2.4 Liquid junction potential

When two adjacent solutions have inequal ion concentrations and mobilities, a liquid junction potential E_l is developed at the interface between them. Ion concentration and mobility differences can be developed between different regions in a liquid. Thus, when biopotentials are measured with two electrodes, E_l can possibly be developed. Adding to that, it can also develop for a single electrode between the electrolyte and body fluid. The liqud junction potential can be calculated based on equation

$$E_l = \left(\frac{u^+ - u^-}{u^+ + u^-}\right) \frac{R_m T}{nF} \ln\left(\frac{c_1}{c_2}\right) \tag{2.6}$$

where u^+ and u^- are the ionic mobilities of positive and negative ions, respectively, R_m is the molar gas constant, T is the absolute temperature, n is the valence of the involved ion, F is the Faraday constant and c_1 and c_2 are the adjacent ion concentrations [13].

Liquid junction potentials have lower values than half-cell potentials in general. For instance, when a junction is formed by two sodium-chloride solutions with a tenfold concentration difference, E_l can be as high as 12 mV [13]. In a typical biopotential recording, this is still a significant source of error. Equation 2.6 describes the liquid junction potential of a single electrolyte. Should more electrolytes be involved, the liquid junction potentials should be determined for all of them.

2.2.5 Electrolytic gels

In addition to enabling charge transfer, the usage of electrolytic gels (hereafter referred to as gels) serves other purposes as well. First, the surface of skin is by no means even and homogeneous. The gel increases the actual contact area between skin and electrodes, which results in reduced contact impedance. Adding to that, the gel tends to diffuse to skin which also tends to reduce the contact impedance. Furhermore, hair would also make it more difficult to create a good contact between electrodes and skin without the use of gel. Finally, the use of gels also provides an interface which allows minor movements of the electrode without a loss of contact.

Electrical conductivity of a gel is defined by its concentration of ionic salts. The major part of ions in tissue consists of sodium, potassium and chloride ions. Consequently, gels usually contain sodium chloride and potassium chloride in order to ensure biocompatibility. However, there are also some chloride-free gels. In addition, some gels contain abrasives such as pumice or quashed quartz which cause enhanced penetration of upper skin layers when rubbed against skin. [1]

2.3 Electrode-skin interface

Electrode contact impedance quantifies the property of the electrode-skin contact to oppose time-varying electric current. It is ofter measured prior to biopotential recording to assess the quality of the electrode contact. The electrical behavior of the electrode contact can be analyzed using an equivalent electric circuit model. For the sake of clarity, the electrode contact is divided to two components; the metal-electrolyte interface and the electrical model of skin. The metal-electrolyte interface can be studied quite easily in practice by placing two electrodes face-to-face with gel between them. Studying the effects of skin is more complex, as metal-electrolyte interfaces are always needed for the study. Adding to that, signals originating from muscle activity are likely to be present.

2.3.1 Metal-electrolyte interface

An equivalent electric circuit model of the metal-electrolyte interface is presented in Fig. 2.2. As discussed in section 2.2, the charge distribution causes a the half-cell potential over the interface. This is denoted as E_{hc} in the figure. As also mentioned in the previous section, the double layer acts like a capacitor. Thus a capacitor C_d is included in the model. The double layer dimensions are of a molecular scale (10^{-10} m) which results in a high capacitance value of the double layer [13,14].

It is also known that direct current can pass through the metal-electrolyte interface. Therefore a parallel resistance R_d is also included in the model. R_d represents the leakage resistance across the double layer. The values of both R_d and C_d are dependent on frequency and current density. A resistance R_s is also included in the model, representing the interface effects and the resistance of the electrolyte. [12]

Various other models for the interface have also been suggested. References such as [13,15,16] are suggested for the interested reader. However, in the context of this thesis, the model presented in Fig. 2.2 is sufficient.

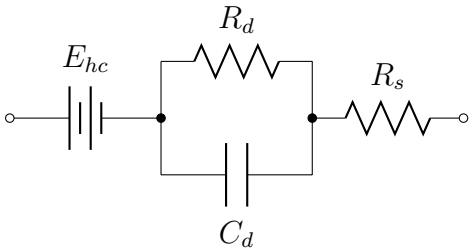

Figure 2.2. *Metal-electrolyte interface equivalent circuit model. [12]*

2.3.2 Anatomy of skin

An illustration of anatomy of skin is presented in Fig. 2.3. Skin consists of epithelial tissue. There are three layers in skin that are called *epidermis, dermis* and subcutaneous

layer (also called fatty tissue as in the figure). The outermost layer, *epidermis*, acts as a barrier protecting underneath tissue against the outside environment. It contains several sublayers of which *stratum basale* is the innermost one where cells are multiplied. Multiplied cells are transported upwards to the surface of skin. During the transportation they undergo changes. Finally they end up in *stratum corneum* which is the outermost sublayer, as compacted, flattened, nonnucleated and dehydrated cells. The replacement process of these dead cells by cells transported from inner sublayers it continuous. The thickness of *stratum corneum* can be as small as $10\,\mu m$. However, at the sole of the foot, thicknesses of more than $1\,mm$ are possible. The composition of *stratum corneum* is highly inhomogeneous. Hair follicles and sweat ducts pass through *epidermis*, and melanocytes are located in it. [1,17]

The second layer, *dermis*, is formed from a dense network of connective tissue. This tissue consists of collagen fibers, thus providing skin with elastical properties and strength. *Dermis* contains blood vessels, hair follicles, sweat glands and oil glands. Underneath it is the subcutaneous layer which consists of structures of connective tissue, thus enabling skin to move freely with respect to underlying bone structures on most parts of the body. It is also an area for fat storage. Adding to that, it also protects organs beneath the skin. [1]

The thickness of *stratum corneum* of the same body site varies between individuals [18]. Generally, subjects with dark skin have denser *stratum corneum* layers which contain more cells than subjects with fair skin. This leads to lower skin capacitances and higher impedances for dark-skinned subjects. However, the thickness of *stratum corneum* does not vary with age. Additionally, there appears to be no gender differences. [1] An increased hair follicle density decreases the resistance of skin. Hair follicle density can vary between 40 and $70\,cm^{-2}$ [19]. Consequently, electrical properties of skin can vary significantly between different subjects and body sites.

Resistance of skin is also affected by presence and activity of sweat glands. The density of sweat glands is dependent on the body site. For instance, on palms of hands the density is approximately $370\,cm^{-2}$. However, at forearm the density is approximately $160\,cm^{-2}$. The sweat duct diameter can also vary between 5 and $20\,\mu m$. As a result, skin resistance can be time-dependent based on activity of sweat glands. [1] Blood circulation is also likely to have an effect on the electrical properties of skin, especially during physical activity. For the sake of simplicity, its effects are usually neglected.

2.3.3 Electric circuit model of skin

An example equivalent electric circuit model of skin is presented in Fig. 2.4. *Epidermis* can be considered as an ionically semi-permeable membrane. This results in a difference of ion concentrations across the membrane, which according to the Nernst equation causes a potential difference [12]. This potential difference is also known as the transepithelial potential which is the sum of all cell membrane potentials in the epithelial tissue layer.

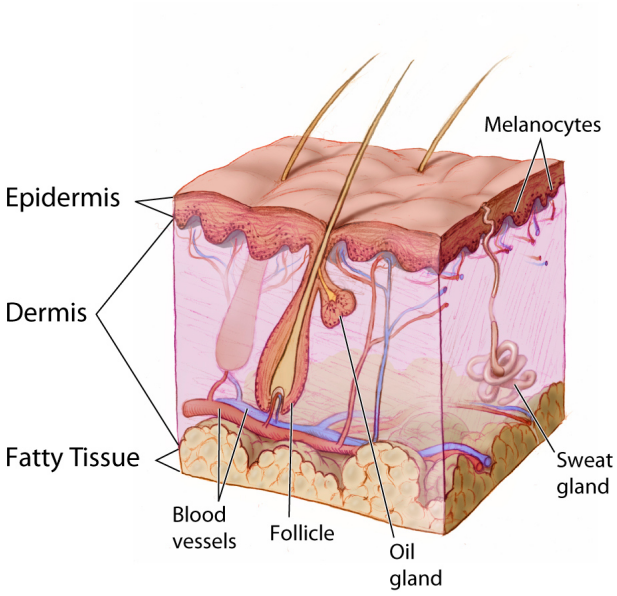

Figure 2.3. *Illustration of anatomy of skin. [20]*

The skin potential is denoted by E_{se} in Fig. 2.4.

The dead skin cells of *stratum corneum* are a relatively dielectric medium. As a result, its impedance is high. However, capacitive coupling through *stratum corneum* between a conductive metal electrode and the conductive tissues underneath is possible [1]. Therefore the model contains a capacitor C_e. It is also known that the impedance of *epidermis* behaves like a parallel RC circuit [12]. Therefore a resistor R_e is also included in the model. Skin impedance formed by R_e and C_e is the largest component of the impedance of the whole electrode-skin interface [1]. *Dermis* and subcutaneous layer are more conductive media and generally behave as pure resistances [12]. Thus they are represented only with a resistor R_u.

Sweat glands secrete fluid which contains ions. The ion concentrations of the fluid differ from those of extracellular fluid, which results in a voltage E_p appearing between a lumen of a sweat duct and *dermis* and subcutaneous layer. The parallel connection of R_p and C_p is due to the wall of sweat gland and duct. In resting conditions, sweat glands are minimally active so their effect can be neglected in most cases. [12]

According to McAdams [1], there have been several observations of regional differences of skin impedance in the low-frequency range, which is dominated by R_e [21–23]. Therefore, variations of skin impedance between sites and subjects tend to be due to large variations of R_e.

Ackmann and Seitz [24] have stated, according to Grimnes and Martinsen [17], that as a rough guideline the impedance of skin is mostly determined by *stratum corneum* at frequencies below 10 kHz. On the other hand, at higher frequencies it is mostly de-

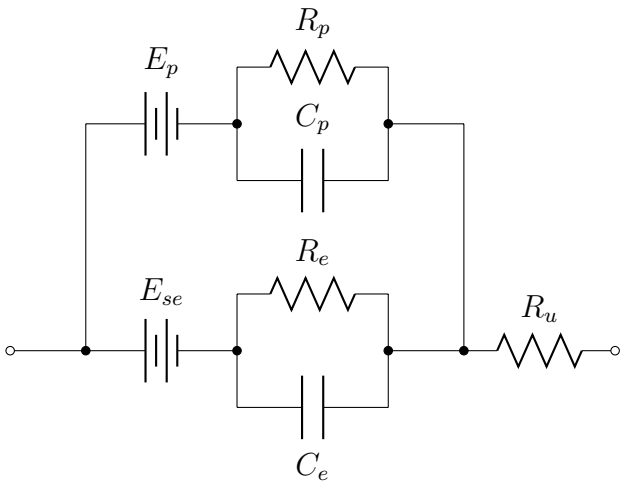

Figure 2.4. *An example equivalent electric circuit model of skin. E_p, R_p anc C_p are typically ignored in resting conditions. [12]*

termined by viable skin. According to a finite element simulation by Martinsen et al., *stratum corneum* accounts for only about 10% of skin impedance at 100 kHz. At 10 Hz, however, *stratum corneum* accounts for about 98% of skin impedance. [25]

2.3.4 Skin preparation

There are a variety of techniques used for preparation of skin. Wiping the skin with alcohol removes some of the loose cells of *stratum corneum* and poorly conducting lipid surfaces from the top of epidermis. Another technique is stripping which means repeatedly applying and removing an adhesive tape to and from the skin which removes cells from *stratum corneum*. Yet another technique is skin abrasion with for instance a sand paper. Skin can also be punctured with a needle or a sharp tip. Even a shallow puncture can provide a low-resistance pathway through skin [26]. All these techniques tend to short out E_{se}, C_e, and R_e [12]. De Talhouet and Webster have presented data which shows the electrode contact impedance to decrease relatively linearly as a result of repeated stripping with an adhesive [4].

After skin is abraded, some time is needed for the skin to recover. Tam and Webster have assessed skin regrowth based on measured skin offset potentials. According to their results it took 1–2 days for skin abraded 20 times to recover [3]. Consequently, during long-term EEG monitoring it is possible that skin recovery has an effect on electrode contact impedances.

Removal of *stratum corneum* exposes the deeper layers of skin and makes them more susceptible to sources of irritation, such as the electrode, the gel and possible adhesives used for electrode attachment. The higher the salt concentration of a gel is, the more likely it is to cause irritation. Irritation can cause redness, itching, swelling and even pain on the skin. Adding to irritation caused by external sources, a too strong skin abrasion

can itself cause bleeding and pain.

Electrodes may come into contact with blood products when skin is abraded. As a result, a risk of an infection with a blood-born pathogen exists [27]. According to guidelines of The Unites States Centers for Disease Control, equipment and devices that penetrate tissue should be sterilized before use. However, should electrodes be placed on intact skin, desinfection prior to usage would be sufficient. [28]

2.4 Noise, artifacts and interference

As mentioned earlier, the undesired signals obscuring biopotential measurement consist of noise, artifacts and interference. Table 2.3 presents different undesired signals present in a typical biopotential recording. In this thesis, noise refers to random voltage fluctuations with a more or less Gaussian amplitude distribution. Non-recurring voltage fluctuations are classified as artifacts. Interference includes continuous and repetitive voltages which originate from outside the measurement system. However, this division is not unequivocal as there can be overlap between the terms.

Electrode contact impedance is relevant considering signal quality as it is related to some of the undesired signals. Thermal noise generated at the electrode contact is proportional to the resistive part of the electrode contact impedance. However, total noise generated at the electrode contact is generally significantly larger than expected thermal noise, as has been reported in various articles [2,29–31]. Furthermore, electrode contact impedances are also related to capacitively coupled interference and motion artifacts [3,4,32]. It is generally accepted that signal quality is improved by decreasing electrode contact impedances by skin preparation. According to EEG guidelines, low-frequency electrode contact impedances should be less than five kilo-ohms and equal [33,34]. However, it has been suggested that based on modern engineering principles, EEG signals of a good quality can be recorded with higher electrode contact impedances as well [27].

2.4.1 Quantification

When a continuous and irregular signal $x_c(t)$ is examined, in order to deal with it quantitatively it is usually expressed as a root mean square (RMS) value X_c for a certain averaging

Table 2.3. *Undesired signals in biopotential recording. The items on the same rows are not related to each other.*

Noise	Artifacts	Interference
Thermal noise	Motion artifacts	Capacitive coupling
Metal-electrolyte noise	Other bioelectric events	Inductive coupling
Electrolyte-skin noise		Electromagnetic radiation
Amplifier noise		

time interval ΔT. The RMS value is defined by equation

$$X_c = \sqrt{\frac{1}{\Delta T}\int_0^{\Delta T} x_c^2(t)dt} \tag{2.7}$$

The squared RMS value X_c^2 is called the mean square value and it represents the average power of $x_c(t)$ dissipated in a $1\,\Omega$ resistor.

Continuous signals are approximated with discrete signals, that is with a set of measured values. The RMS value X_d of a discrete signal $x_d(n)$ is defined by equation

$$X_d = \sqrt{\frac{1}{N}\sum_{i=0}^{N} x_d^2(n)} \tag{2.8}$$

where N is the number of samples used for averaging. As is the case with continuous signals, the squared RMS value X_d^2 represents the average power of $x_d(t)$ dissipated in a $1\,\Omega$ resistor. In statistical terms, when the mean value μ of a data set is zero, the standard deviation σ of the data set equals its RMS value.

Another useful property in the study of random signals is power spectral density (PSD). PSD provides information of how power of a signal is distributed with frequency. PSD can be calculated using the so-called direct approach by equation

$$\text{PSD}(f) = |X_k|^2 \tag{2.9}$$

where X_k is the discrete Fourier transform (DFT) of signal $x_d(n)$ [35]. DFT is defined by equation

$$X_k = \sum_{n=0}^{N-1} x_d(n)e^{-j\frac{2\pi nk}{N}} \tag{2.10}$$

where N is the number of samples, j is the imaginary unit, and $k = 0, \ldots, (N-1)$. When the studied signals are voltages, the units $\text{V}^2\,\text{Hz}^{-1}$ or $\text{dB}\,\text{Hz}^{-1}$ are used for PSD. Manufacturers of integrated circuits usually specify component noise properties as spectral noise densities, which is the square root of PSD, and has a unit $\text{V}\,\text{Hz}^{-1/2}$.

2.4.2 Thermal noise

Thermal noise is present in all passive resistive elements. Thermal noise is intrinsic and it occurs due to thermal fluctuations of charge carriers. Thermal noise is not dependent on voltage. The presence of thermal noise can be seen by measuring RMS voltage over a resistor without any voltage source, although it must be assumed that interference sources are removed in this experiment.

Thermal noise is approximately equal to white noise which means that its PSD is nearly

constant throughout the whole frequency spectrum, and the probability density function of its amplitude is nearly Gaussian. Thermal RMS noise voltage of an element with resistance R is quantified by equation

$$V_{th} = \sqrt{4k_bTR\Delta f} \tag{2.11}$$

where k_b is the Boltzmann constant, T is the absolute temperature and Δf is the examined frequency bandwidth. Theoretically, the minimum noise level of any conductor is its thermal noise.

2.4.3 Metal-electrolyte noise

The variation of half-cell potential E_{hc} contributes to noise generated at the interface. Other components affecting the interface noise are thermal noise of the resistive part of metal-electrolyte interface impedance, noise resulting from mechanical vibrations at the interface, and noise resulting from non-stationary electrochemical reactions [31]. Metal-electrolyte noise cannot usually be distinguished from amplifier internal noise. [2,31]

Gondran et al. have reported peak-to-peak metal-electrolyte noise values of $0.3\,\mu V$ at a bandwidth of $\Delta f = 0.5$–$100\,Hz$ with pre-gelled Ag-AgCl electrodes [29]. This value has been defined with with cross-correlation method using two independent measuring channels, which eliminates the contribution of amplifier noise. The peak-to-peak value can be converted to RMS value if the noise is assumed to be Gaussian. The instantaneous value of Gaussian noise is within 6.6 standard deviations of the RMS value for 99.9% of the time [36]. Thus, the $0.3\,\mu V$ peak-to-peak value can be approximated as an RMS value of $45\,nV$. The value is reportedly larger than theoretical thermal noise, so excess noise was present within the abovementioned frequency bandwidth [29].

Fernández and Pallás-Areny have found the metal-electrolyte noise to be more than 10 times higher than the expected thermal noise for pre-gelled Ag-AgCl electrodes (Red Dot, 3M Company, St. Paul, MN, U.S.A.). Metal-electrolyte noise also decreased with increasing frequency. Its RMS value was less than $1\,\mu V$ in the frequency bandwidth of $\Delta f = 0.5$–$500\,Hz$. At frequencies below $10\,Hz$, decreased electrode area increased the noise. Noise was also found to depend on used gel at the same frequencies. Additionally, electrode half-cell potential was found to be a good indicator of metal-electrolyte noise. [30]

Huigen et al. have found a long stabilization time to reduce metal-electrolyte noise to a negligibly small magnitude. The stabilization time varies with different electrode materials, but eventually all materials will reach the same level of noise. Electrodes with the shortest possible stabilization time are the most practical. [2]

2.4.4 Electrolyte-skin noise

Noise generated at the electrolyte-skin interface remains a topic which is not well known. Previous studies have revealed that the interface noise is generally higher than the equivalent thermal noise associated with the resistive part of of the interface impedance. Both Huigen et al. and Horikawa et al. have concluded that the total electrode noise originates mainly from the electrolyte-skin interface [2,31]. The study of the electrolyte-skin interface is difficult as signals originating from muscle activity are likely to be present.

The voltage E_{se} over *epidermis* presented in Fig. 2.4 is substantial compared to magnitude of EEG signal. Tam and Webster have reported values such as $-10\,\mathrm{mV}$ for upper arm and $-64\,\mathrm{mV}$ for palm. By abrading skin, the E_{se} can be reduced. [3] Clochesy et al. have also reported the same result [37]. Variations of V_{se} contribute to electrolyte-skin noise. Skin abrasion is likely to reduce the magnitude of voltage variations, which results in less noise.

Gondran et al. have found the whole electrode-skin interface noise to correspond with thermal noise at frequencies over $100\,\mathrm{Hz}$. However, at frequencies below $100\,\mathrm{Hz}$, excess noise is evidenced. The peak-to-peak fluctuations caused by the excess noise can be 50 to $60\,\mu\mathrm{V}$. The noise could also be diminished by decreasing electrode contact impedance. Increasing the electrode area was found not to decrease the excess noise. Two possible reasons for the excess noise are non-equilibrium processes in *stratum corneum*, and the ionic nature of skin which could result in fluctuations of ion concentration and mobilities. [29] These fluctuations would result in liquid junction potential variations.

Horikawa et al. have reported the presence of excess noise at frequencies from 1–$1000\,\mathrm{Hz}$. The origin of the excess noise are unclear, but non-stationary and out-of-equilibrium processes are suggested in their article too. [31]

Fernández and Pallás-Areny found the total electrode-skin interface noise to be 10 times higher than the expected thermal noise for wet-gel electrodes $10\,\mathrm{cm}$ apart on inner forearm. For a bandwidth of $\Delta f = 0.5$–$500\,\mathrm{Hz}$, the RMS noise voltage ranged from 1 to $15\,\mu\mathrm{V}$ depending on subject, electrode type and body site. Electrode area had no significant effect on total electrode-skin noise. The increased effect of EMG on larger electrodes is suggested to compensate the effect of reduced impedance on the noise. [30]

However, Huigen et al. have found the magnitude of electrode noise to be inversely proportional to the square root of the electrode area on the skin. They also state that electrode noise is highly dependent on the used electrode gel and skin properties of the test subject. After application, the noise of wet-gel Ag-AgCl electrodes decreased and reached a stable value after approximately 20 minutes. [2]

Huigen et al. also studied the relationship between electrode contact impedance at DC and contact noise magnitude of wet-gel electrodes, and found a relationship in both inter- and intra-individual data. However, a physical explanation for this relationship could not

be provided. By decreasing impedances with skin abrasion, noise magnitude could be decreased up to 80%. [2]

2.4.5 Amplifier noise

All semiconductors exhibit inherent noise which is due to generation and recombination of electron-hole pairs [36]. These phenomena are random in nature, and therefore also inherent noise of amplifiers is random.

Operational amplifier noise can be modelled with two uncorrelated noise sources, a voltage source v_n and a current source i_n at the input of a noiseless operational amplifier. A model with this representation is presented in Fig. 2.5. Z_s represents the input source impedance. The total noise is the root of sum of squares of the uncorrelated noise sources, so the total voltage input noise voltage v_{in} can be quantified as

$$v_{in} = \sqrt{v_n^2 + Z_s^2 i_n^2} \tag{2.12}$$

From the equation it can be seen that by reducing Z_s, the total input noise can be reduced. In a practical situation, v_n can be measured by short-circuiting the input terminals of the op amp and measuring the output voltage v_o, and then dividing it with the voltage gain of the amplifier. i_n can be measured by connecting a resistor with a known value of resistance between the amplifier input terminals and measuring v_o. Again v_o must be divided with the voltage gain of the amplifier. Both v_n and i_n have the same characteristics. At low frequencies they are characterized as 1/f noise, and at high frequencies as white noise [36]. In biomedical applications, amplifiers with very low input noise currents are desired as this way the amplifier noise is independent of source impedance. As a result, the effect of input noise current can usually be neglected. In a realistic amplifier, thermal noise of all circuit resistors contributes to total noise.

2.4.6 Motion artifacts

Motion artifacts can be caused by movement of metal with respect to electrolyte, stretching or deformation of skin and movement of electrode wires. The movement of metal with respect to electrolyte causes temporary changes in the electrical double layer which results in half-cell potential variations [38]. After the movement of metal with respect

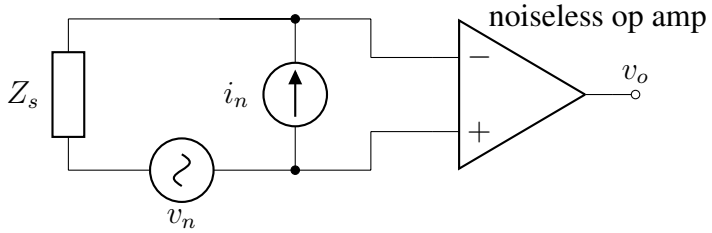

Figure 2.5. *Noise model of an operational amplifier.*

to electrolyte, a stabilization process occurs until the interface is at a state of equilibrium again. Ödman and Öberg report based on experimental data that reduction of electrolyte resistivity, polarization potential and electrode movement velocity all reduce motion artifacts [39]. Tam and Webster have observed no significant offset potential variations due to squeezing and separating two recessed electrodes with gel in between as long as the gel bridged the two electrodes. Consequently, the metal-electrolyte interface is not a major source of motion artifacts with recessed electrodes. [3]

Ödman and Öberg have reported that artifacts from 400 to $600\,\mu V$ can be caused by movement of gel parallel to skin surface [39]. These variations are caused by liquid junction potential variations at the electrolyte-skin interface [39,40].

Skin stretching and deformation cause changes in skin offset voltage E_{se}. Tam and Webster found vertical deformation to cause voltage variations in the range of 5–$10\,mV$ on forearm. With horizontal deformation the variations were about half of those values. In conclusion, skin deformation is the most important source of motion artifacts. Skin abrasion was found to decrease the offset potential variations. [3] De Talhouet and Webster have found the offset potential variations to decrease linearly with decreasing electrode contact impedance below impedance values of $80\,k\Omega$ measured at $13\,Hz$. For higher impedances, the offset potential varied significantly. [4]

Movement of insulated electrode wires and their deformation can cause triboelectric noise which can induce artifacts [41]. The best way to minimize these artifacts would be to attach the cables firmly. The usage of stiff cables would also serve this purpose.

2.4.7 Other bioelectric events

When muscle cells are electrically or neurologically active, they produce potential fluctuations. Electromyogram (EMG) is the signal originating from muscle activity. In EEG, however, EMG is usually considered an undesired artifact, as it can severely disturb the desired signal. Thus, minimal muscle activity during recording is desired. In general, most of EMG signal power lies at frequencies between 20 and $200\,Hz$ [42]. Consequently, overlap between EMG and EEG signals exists. When properties of the electrode-skin interface are studied, body sites with a minimal amount of muscles in the vicinity should be used.

A steady potential from cornea to retina exists. Therefore the eyeball can be thought of as a dipole. [10] As a result, movement of the eye results in potential fluctuations in electrodes in the vicinity of the eye. The signal produced by eyeball movements is called electro-oculogram (EOG). Electric fields originating from the heart can be conducted to scalp, which results in an ECG artifact. Adding to that, an electrode placed on a pulsating vein will also result in an artifact originating from the heart. However, in this case the artifact might as well be classified as a motion artifact.

2.4.8 Capacitive coupling

A changing electric field can cause displacement currents to flow through the measurement system to earth. The displacement currents are coupled via parasitic capacitances, hence the term capacitive coupling. According to Ohm's law, a voltage is induced based on the magnitude of current and impedance of the conducting system. In the case of bioelectric measurements, displacement currents can be coupled to the electrode wires, the patient and the amplifier. A setup clarifying capacitive coupling in ECG is presented in Fig. 2.6. However, the same principles apply to EEG. In this setup, the patient is isolated from earth.

The displacement currents are coupled to electrode wires through capacitances C_{ca} and C_{cb}. It can be assumed that the amplifier input impedances Z_{ia} and Z_{ib} are very large, so the resulting currents i_a and i_b flow to the patient via electrode contact impedances Z_{ea} and Z_{eb}, and from the patient to earth via C_{body} and via the series connection of Z_{rl} and C_{iso}. The resulting voltage v_{ab} at the amplifier input is

$$v_{ab} = i_a Z_{ea} - i_b Z_{eb} = i Z_e \left(\frac{\Delta Z_e}{Z_e} + \frac{\Delta i}{i} \right) \tag{2.13}$$

where $Z_e = \frac{1}{2}(Z_{ea} + Z_{eb})$ and $i = \frac{1}{2}(i_a + i_b)$ [32].

In EEG, the electrodes are spaced relatively closely and the electrode wires are of approximately same length, so the displacement currents are likely to be nearly of the same magnitude. This emphasizes the importance of balanced electrode contact impedances, as the more balanced they are, the smaller is the effect of capacitive coupling. In practice, most capacitive coupling occurs through electrode wires. [32,43]

A displacement current i_1 is coupled from mains power to the body via C_{pow} and flows through it to earth via C_{body}. When the patient is connected to an amplifier, a part of i_1 will flow to earth through Z_{rl} which is the electrode contact impedance of the ground electrode. As a result, a voltage between the patient and amplifier common is generated. This voltage is called common-mode voltage, denoted v_{cm}. Should the patient not be grounded, the pathway from patient to amplifier common would consist of electrode contact impedances and amplifier input impedances, which would result in a significantly larger value of v_{cm}.

In the configuration presented in Fig. 2.6, the grounding is implemented passively, meaning that the ground electrode is connected directly to amplifier common. However, common practice is to use an active grounding circuit implemented with an operational amplifier, called driven-right-leg (DRL) circuit. It senses the the average voltage from the amplifier inputs (which is v_{cm}), inverts and amplifies it, and feeds it back to the patient. This is an effective way of reducing v_{cm}. Additionally, it also creates a large-impedance pathway between patient and earth which improves safety in experimental

situations where a proper patient isolation is not feasible.

A potential divider is formed by both Z_{ea} and Z_{ia}, and Z_{eb} and Z_{ib}, respectively. This causes a differential voltage v_{ab} at the amplifier input which is quantified by equation

$$v_{ab} = v_{cm}\left(\frac{Z_{ia}}{Z_{ia}+Z_{ea}} - \frac{Z_{ib}}{Z_{ib}+Z_{eb}}\right) \tag{2.14}$$

If assumed that Z_{ia} and Z_{ib} are significantly larger than Z_{ea} and Z_{eb}, the equation can be rewritten as

$$v_{ab} = v_{cm}\frac{Z_e}{Z_i}\left(\frac{\Delta Z_e}{Z_e} + \frac{\Delta Z_i}{Z_i}\right) \tag{2.15}$$

where $Z_e = \frac{1}{2}(Z_{ea} + Z_{eb})$ and $Z_i = \frac{1}{2}(Z_{ia} + Z_{ib})$. Thus, v_{cm} is converted to differential mode voltage. The larger v_{cm}, Z_e/Z_i and the imbalances of electrode contact and amplifier input impedances are, the stronger is the effect. [32]

A displacement current i_2 is also coupled via C_{sup} to the amplifier common. In an isolated measurement, i_2 flows from amplifier common to earth partially via C_{iso} and partially via the series connection of Z_{rl} and C_{body}. The part of i_2 which flows through the body contributes to v_{cm}. [32]

In conclusion, changes and imbalances of electrode contact impedances degrade the signal quality by increasing capacitive coupling through the electrode-amplifier interaction. Electrode contact impedances can be balanced with a meticulous skin preparation accompanied with measurement of contact impedances. By using amplifiers with extremely high input impedances, the effect of contact impedance changes over time can be minimized.

2.4.9 Inductive coupling

In inductive coupling a changing magnetic field in the vicinity of a conductor loop induces a voltage in the loop. The induced voltage v_M can quantified by equation

$$v_M = 2\pi f A B \tag{2.16}$$

where f is frequency, A is the area of the conductor loop, and B is the vector component of the flux density of the magnetic field oriented perpendicular to the loop surface [27]. The effect of inductive coupling may add or cancel based on how the magnetic field is oriented with respect to inductive conducting loops. In a typical biopotential recording, the magnetic fields originate from transformers of equipment power supplies.

Based on equation 2.16, it is clear that by minimizing the areas of conductor loops the effect of inductive coupling can be minimized. In practice this is best done by twisting the electrode wires up to the body, and running them close to the body [43]. In EEG this is relatively easy to accomplish as the electrodes are relatively closely spaced compared to

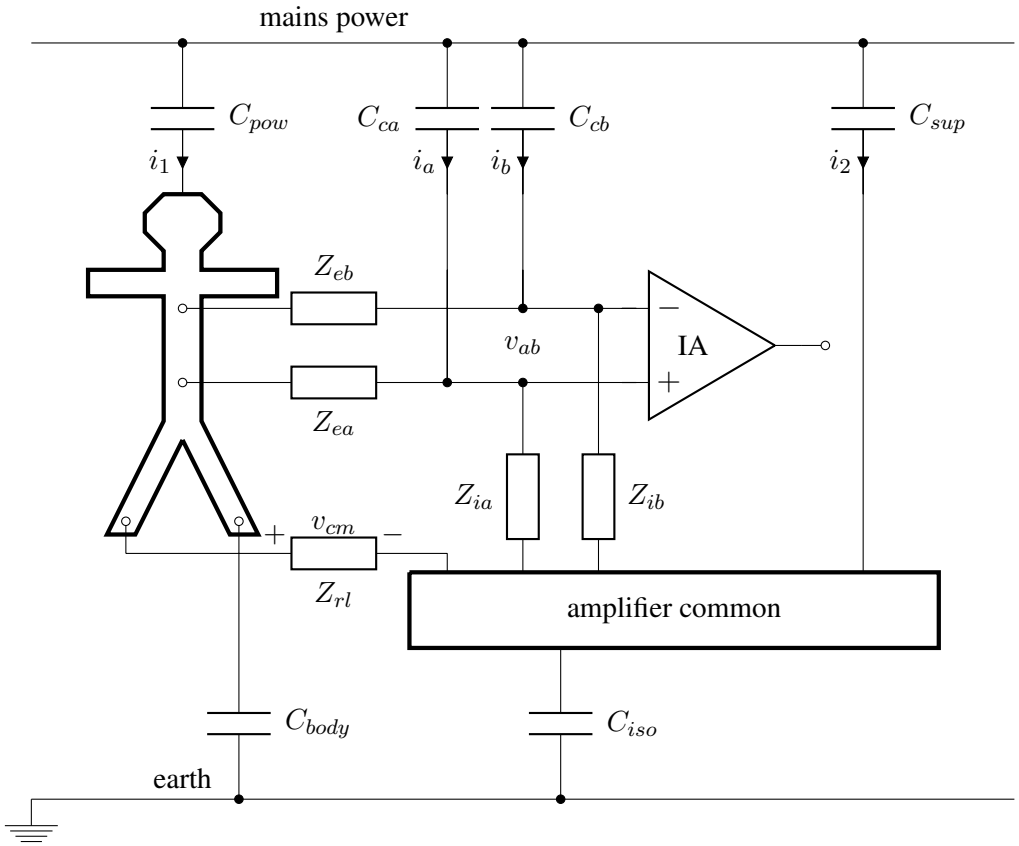

Figure 2.6. *An illustration of capacitive coupling in ECG. Adapted from Metting van Rijn et al. [32].*

ECG for instance. Shielding the sources of magnetic fields with ferromagnetic materials and keeping them as far away as possible from the patient is also effective [32]. With these precautions, inductive coupling has a very small effect in EEG.

2.4.10 Electromagnetic radiation

Radiation from nearby illumination sources for instance can also induce voltages in the measurement system which contribute to v_{cm}. However, a radiation induced interference voltage might not always be induced as a common-mode voltage to the measurement system. An illustrating example is a situation where a nurse touches an electrode during EEG recording. In this case the voltage induced to the body of a nurse through radiation is connected to a single electrode which results in an interference voltage seen at the amplifier output.

High frequency or radio frequency (RF) interference can originate from hospital equipment such as electrosurgical units or x-ray machines. Adding to that, nearby high-power radio, television or satellite facilities can also cause interference due to radiation. The p-n junctions of all semiconductors tend to rectify RF signals. Hence a DC offset is induced. [44]

2.5 Biopotential amplifiers

The most important functional blocks of a biopotential amplifier analog front-end are presented in Fig. 2.7. The electrode-skin signal source together with the amplifier input characteristics are both critical for successful EEG recording. Therefore the functional blocks relevant to this thesis are input protection and filtering, and input stage. This section will provide an analysis of these blocks and the implications of electrode-skin contact to them. A detailed description of biopotential amplifier functions is given by Neuman [44].

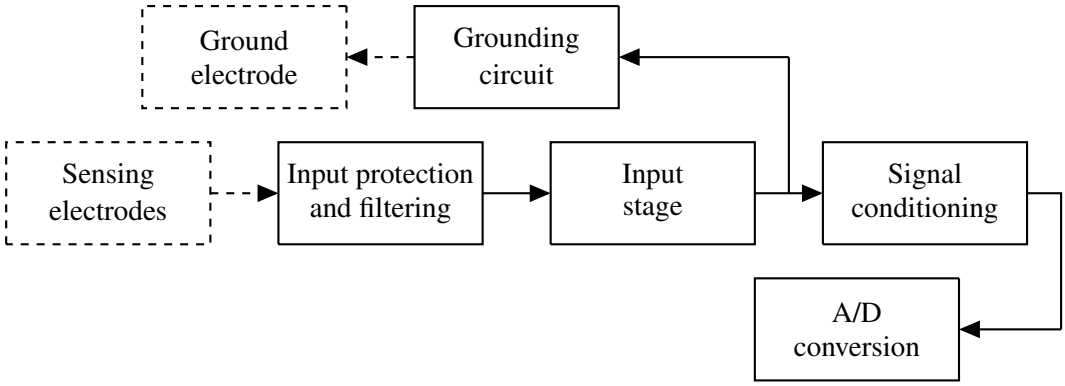

Figure 2.7. *A block diagram of a biopotential amplifier analog front-end.*

2.5.1 Input protection and filtering

Biopotential amplifiers can be damaged if a high-voltage transient occurs between its input terminals. A possible source of such a transient is patient defibrillation. Therefore the amplifier inputs are protected by inserting voltage-limiting devices between input and ground terminals. As long as the input voltage remains below a threshold value, the voltage-limiting device is practically non-conducting and therefore appears as an open circuit, thus not affecting the amplifier input impedance. Should the input voltage exceed the threshold value, the current-limiting device begins to conduct current so that the input voltage remains below the threshold value.

Three types of voltage-limiting devices are normally used: diodes, Zener diodes and gas-discharge tubes. With two diodes connected in parallel, the threshold voltage is about $600\,\mathrm{mV}$. A higher threshold voltage can be achieved by connecting multiple diodes in series. Even higher threshold voltages, approximately from 2–$20\,\mathrm{V}$ are achieved by connecting two Zener diodes back-to-back. With gas-discharge tubes, the threshold voltages are in the range from 50–$90\,\mathrm{V}$. [44] In Fig. 2.8, two back-to-back Zener diodes are connected from both channel inputs to amplifier common. v_{bio} is the voltage sensed by the electrodes.

By adding low-pass filters to the amplifier inputs, DC offset originating from RF interference can be attenuated. The filters are formed by resistors R in both channel inputs,

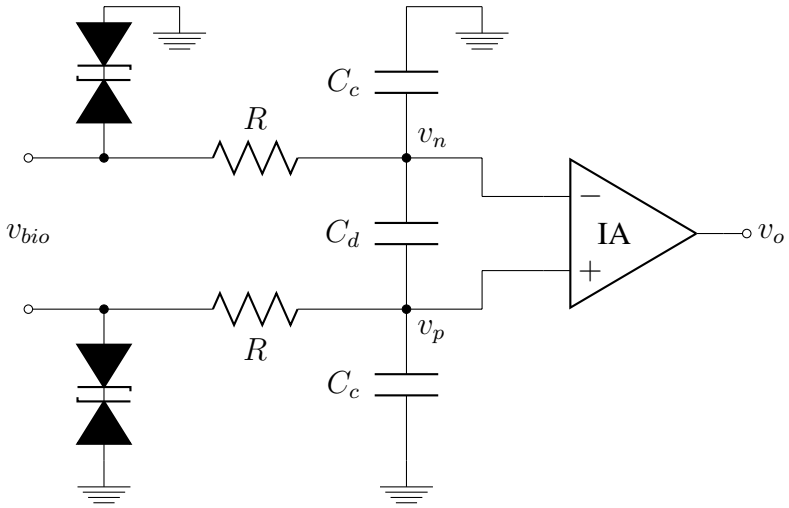

Figure 2.8. *A circuit for input protection and filtering.*

a capacitor C_d connected between the inputs, and capacitors C_c connected from both inputs to amplifier common, all presented in Fig. 2.8 also. This particular implementation results in two cut-off frequencies; f_d for differential interference signal, and f_{cm} for common-mode interference signal. The cut-off frequencies are defined by the following equations [45].

$$f_d = \frac{1}{2\pi R\left(2C_d + C_c\right)} \tag{2.17}$$

$$f_{cm} = \frac{1}{2\pi R C_c} \tag{2.18}$$

With this implementation, C_d affects the amplifier differential input impedance. It's value should be kept relatively small, supposedly in the range of hundreds of picofarads to minimize its effect on input impedance at frequencies of EEG signal [44]. Adding to that, capacitors C_c affect amplifier common-mode input impedance.

2.5.2 Input stage

The input stage consists of an istrumentation amplifier (IA). An IA has the following characteristics; extremely high input impedance, very low output impedance, accurate and stable gain, and high common-mode rejection ratio (CMRR) [36]. The classic three op amp IA circuit is presented in Fig. 2.9. The two buffer op amps at the input provide an extremely high input impedance. The third op amp amplifies the difference of the input voltages v_p and v_n. The differential voltage gain G_d of the IA depends on the resistor ratios according to the following equation

$$G_d = \left(1 + \frac{2R_3}{R_G}\right)\frac{R_2}{R_1} \tag{2.19}$$

IAs are usually provided as integrated circuits containing all compontents of Fig. 2.9 except resistor R_G. Thus, the gain of the IA can be easily set to a desired value. As discussed earlier in Sections 2.2 and 2.3, offset voltages are generated at the electrode-skin interface. Normally there are differences of the offset voltages between different electrodes. As a result, offset voltages are produced to amplifier inputs. The offsets are generally high compared to the desired signal and they tend to change with time due to polarization. Thus, the input stage should have a low gain to prevent saturation of the amplifier. This is especially relevant in applications where low supply voltages are used. Dynamic input range is a parameter which defines the maximal input voltages that the amplifier can tolerate without saturating.

As mentioned in subsection 2.4.8, common-mode voltage v_{cm}, is always present in bioelectric measurements. IAs amplify the difference of their two input terminals with the set gain. However, a realistic IA will also amplify v_{cm}. The operation of a realistic IA is described by equation

$$v_o = G_d(v_p - v_n) + G_{cm}\left(\frac{v_p + v_n}{2}\right) \tag{2.20}$$

where G_d is the differential voltage gain, G_{cm} is the common-mode gain, and v_p and v_n are the voltages of its positive and negative input terminals, respectively. Note that $(v_p + v_n)/2 = v_{cm}$.

CMRR quantifies the property of the amplifier to suppress common-mode voltage. It is defined as the ratio of differential and common-mode gains.

$$\text{CMRR} = \frac{G_d}{G_{cm}} \tag{2.21}$$

It is common to define CMRR as the ratio of powers of differential and common-mode gains, measured in decibels (dB). This gives us the following equation

$$\text{CMRR} = 10\log_{10}\left(\frac{G_d}{G_{cm}}\right)^2 = 20\log_{10}\left(\frac{G_d}{G_{cm}}\right) \tag{2.22}$$

For the IA circuit presented in Fig. 2.9, $G_{cm} = 1$ provided that resistors R_1 and R_2 have negligibly small tolerances.

2.5.3 Input impedance

The input impedance of an amplifier or IA can be divided to differential and common-mode input impedances, denoted Z_{id} and Z_{icm}, respectively. Z_{id} is the impedance between two input terminals of an amplifier. Z_{icm} is the impedance between amplifier common and shorted input terminals. The input impedances are modeled in Fig. 2.10. When v_p and v_n are shorted, the parallel connection $2Z_{icm}||2Z_{icm}$ yields Z_{icm}. When electrodes are

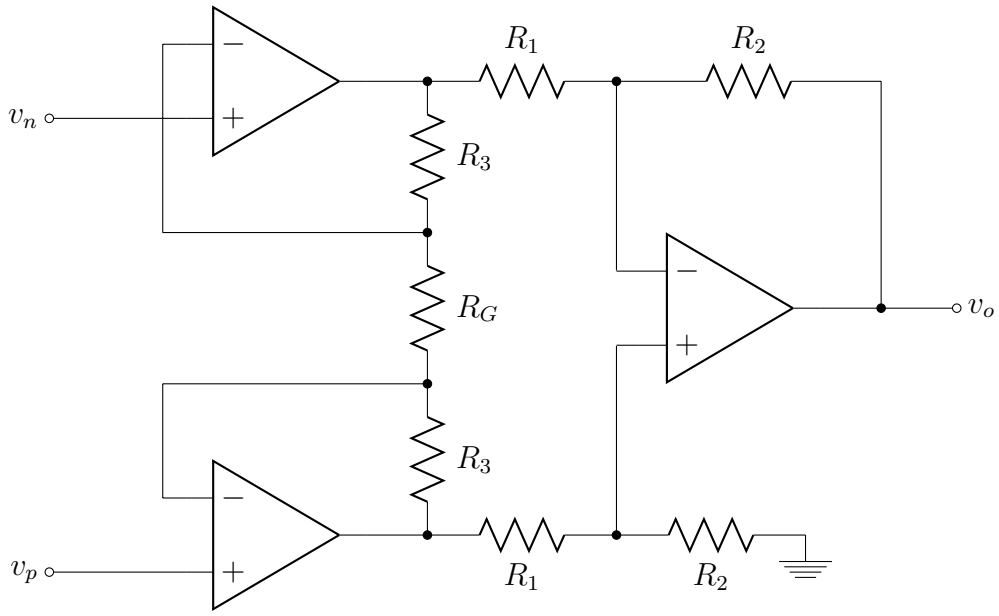

Figure 2.9. *A three op amp instrumentation amplifier circuit.*

connected directly to the IA input, meaning that no input filtering is implemented, the input impedance is defined by the properties of the used IA only. However, should input filtering be used, its effect must also be taken into account.

Usually only the resistive part of the input impedance is specified on data sheets of commercial op amps and IAs. However, in some cases the reactive part is also specified. As an example, for AD620 IA (Analog Devices, Inc., Norwood, MA, U.S.A.) which is a commercial IA typically used in medical instrumentation, both Z_{id} and Z_{icm} are specified as a parallel connection of $10\,\mathrm{G\Omega}$ and $2\,\mathrm{pF}$ [45].

As mentioned in subsection 2.4.8, a potential divider is formed at the amplifier input. In the potential divider, Z_{icm} defines the conversion of common-mode voltage to differential voltage. Its value is generally defined by the amplifier input capacitance at $50\,\mathrm{Hz}$. Z_{id} defines how much the electrode-skin signal source is loaded. Excessive loading of the signal source can alter its characteristics which may result in attenuation and distortion of the signal. Metting van Rijn et al. have suggested that Z_{id} and Z_{icm} should have values of at least $10\,\mathrm{M\Omega}$ and $100\,\mathrm{M\Omega}$ at $50\,\mathrm{Hz}$, respectively [46]. However, these values ensure proper amplifier operation only if electrode contact impedances are of a typical value. Typical values in this context could be in the range of around $10\,\mathrm{k\Omega}$.

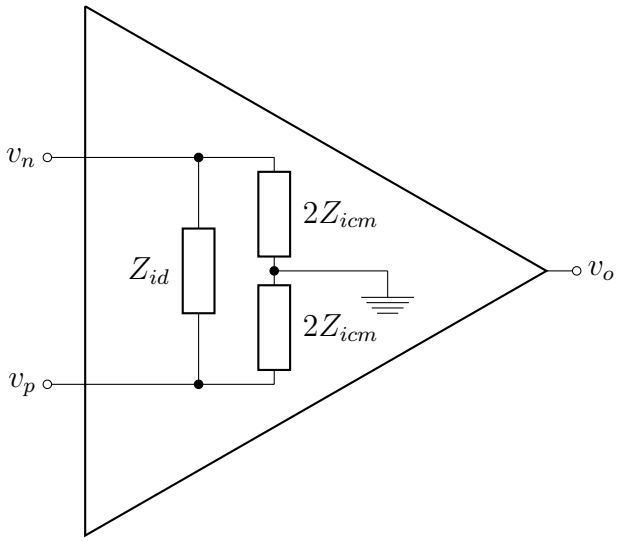

Figure 2.10. *Model of amplifier input impedances. Adapted from Franco [36].*

3. METHODS AND MATERIAL

The relationship of electrode contact impedance and biopotential signal quality was studied in the experimental part of this thesis. The signal quality consists of several factors which were described in the previous chapter. Electrode contact impedance is expected to have a relationship to electrode contact noise which consists of thermal noise generated at the resistive elements of the contact, metal-electrolyte noise and electrolyte-skin noise. Secondly, motion artifact magntitude is also expected to be proportional to electrode contact impedance. Both of these relationships were studied. From other factors contributing to signal quality, also capacitive coupling is related to electrode contact impedances. However, it was not studied as its effect is based on the interaction of the biopotential amplifier input and electrode contact to be more precise. Moreover, practical experiments to study capacitive coupling would require highly specialized instruments and an electrically controlled space.

In the context of the experiments, electrode contact impedance was quantified (and is hereafter referred to) as the magnitude of impedance vector at $20\,\text{Hz}$ frequency. Adding to the experiments related to signal quality, the stabilization of the electrode contact as a function of time was also studied. Finally, the operation of the seizure detection algorithm [5] with noisy signals was studied.

3.1 Measurement equipment

Electrode contact impedances were measured with a circuit consisting of a HP 33120A signal generator (HP/Agilent, Palo Alto, CA, U.S.A.), a $910\,\text{k}\Omega$ bias resistor, and either a Fluke 87 True RMS Multimeter (Fluke Corporation, Everett, WA, U.S.A.) or HP 34410A multimeter (HP/Agilent, Palo Alto, CA, U.S.A.). The signal generator fed a sinusoidal signal of $v_{in}(t) = 5\sin(40\pi t)$ V, thus having a RMS value of $V_{in} = 3.54\,\text{V}$. The circuit schematic is presented in Fig. 3.1 where V_Z is the measured RMS voltage over two electrodes attached to skin (or placed face-to-face with gel in between) and Z_{20} is the magnitude of impedance of the two electrode-skin (or electrode-gel) interfaces at $20\,\text{Hz}$ frequency. Based on Ohm's law, Z_{20} is defined by equation

$$Z_{20} = R\frac{V_Z}{V_{in} - V_Z} \tag{3.1}$$

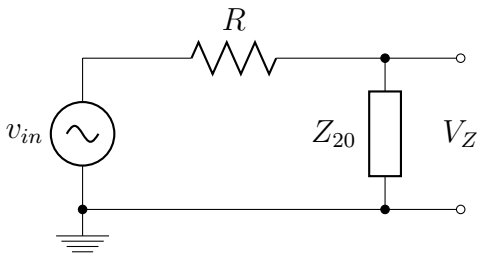

Figure 3.1. *Schematic of the used impedance measurement circuit.*

It is useful to define Z_{20} as the impedance of two electrode contacts instead of defining the individual contact impedances of sensing and reference electrodes, because this way the results can be presented in a clearer manner.

The used electrodes were sintered Ag-AgCl ring electrodes of recessed type (EASYCAP GmbH, Herrsching, Germany). The surface area of the electrodes was $0.84\,\mathrm{cm}^2$. They were attached to plastic ring spacers which were connected to skin with two-sided adhesive rings. The cavity formed under the electrode and inside the ring was filled with gel. Two commercially available gels were used: Abralyt 2000 (EASYCAP GmbH, Herrsching, Germany) and Elefix (Nihon Kohden Corporation, Tokyo, Japan). Abralyt 2000 is an abrasive and chloride-free gel. According to the manufacturer's website, its stable characteristic supports the qualities of sintered electrodes [47]. Elefix is a chloride-containing gel which has been identified to dry relatively slowly which is a favorable characteristic considering long-term EEG monitoring [48].

Two different EEG recording systems were used. A GE EEG system consisted of an N-EEG headbox, E-EEG module, S/5 patient monitor (all GE Healthcare Finland Oy, Helsinki, Finland) and a PC. The signals were sampled at $100\,\mathrm{Hz}$, and the system has an input range of $\pm 400\,\mu\mathrm{V}$. Bandwidth of the system is 0.5 to $30\,\mathrm{Hz}$. The other EEG recording system consisted of a NeurOne EEG system (Mega Electronics Ltd, Kuopio, Finland) and a PC. The system has a default bandwidth of 0.16 to $7000\,\mathrm{Hz}$ without any specially configured filters. In these experiments the signals were filtered with a two-stage filter combination. The first stage was a anti-aliasing low-pass filter, which had an input sampling rate of $80\,\mathrm{kHz}$, an output sampling rate of $10\,\mathrm{kHz}$ and a cut-off frequency of $3\,\mathrm{kHz}$. The second stage was a low-pass filter with an output sampling rate of $500\,\mathrm{Hz}$ and a cut-off frequency of $190\,\mathrm{Hz}$. Input range of the system is $\pm 2.5\,\mathrm{mV}$.

Initially the internal noise voltages V_i of both EEG systems were measured by short circuiting the positive and negative inputs to ground and recording a signal. Due to the more limited bandwidth of the GE EEG systems, its bandwidth from 0.5 to $30\,\mathrm{Hz}$ was used for comparison. The recorded signals were bandpass filtered to that passband with a Fourier filter Matlab function, which is presented as Appendix. The internal noises were found to be $87\,\mathrm{nV}$ and $233\,\mathrm{nV}$ for GE EEG and NeurOne, respectively.

3.2 Electrode contact impedance and noise

All signals recorded in this section were measured with GE EEG system, because it was found to have a smaller level of internal noise at the frequencies of interest. The metal-electrolyte interface noise V_{me} was measured by placing two electrodes electrodes face-to-face in gel with a $5\,\text{mm}$ distance. Adding to that, a ground electrode was based right next to the two electrodes. The metal-electrolyte interface impedance was also measured with the electrodes in the same positions.

Two body sites were selected for the measurements: earlobe and inner forearm. Forearm was selected because of its easy accessibility, and because it has also been used in a previous study [2]. Earlobe was selected because of an assumption that minimal muscle activity is present on this site. Thus, the recorded noise signal would be likely to consist mostly of noise generated at the electrode contact.

On earlobe, the sensing electrodes were placed on opposite sides of the lobule and the ground electrode was placed right next to the earlobe on a site where no hair was present. On forearm, all three electrodes were placed next to each other. During experiments on earlobe, test subjects were in a lying position with a pillow supporting the head, trying to be as relaxed as possible. When experimented on forearm, subjects were sitting with the arm resting on a table.

The actual protocols differed slightly with the two different gels used. With Abralyt 2000, ground electrode area was prepared semi-roughly with a fine sand paper. Areas of the sensing electrodes were not prepared initially. After attachment of electrodes, they were filled with gel. Then Z_{20} was measured and a signal was recorded. Then skin was prepared by rotating and pressing a cotton swab lighty against skin through the electrode center cavity, and gel was added. Then Z_{20} was measured and a signal recorded again. These steps were repeated until Z_{20} was in the order of $10\,\text{k}\Omega$ or less.

Elefix is not an abrasive gel, so proper skin abrasion is not feasible by rubbing the gel against skin through the electrode cavity. Instead, the body site should be prepared before attaching the electrodes. Due to this increased effort needed, only two measurements per subject were performed. The ground electrode site was prepared the same way as mentioned above. For the earlobe measurements, the earlobe was lightly prepared with a fine sand paper initially. Then the electrodes were attached, Z_{20} measured, and a signal was recorded. The next step was removal of the measuring electrodes, which was followed by wiping the skin with alcohol and addiotional light abrasion. Again the electrodes were attached, Z_{20} was measured, and a signal was recorded. For the forearm measurements, two pairs of measuring electrodes were attached right next to the ground electrode. Prior to attachment, the two sites were prepared semi-roughly and roughly, respectively. Then Z_{20} was measured for both electrode pairs, which was followed by simultaneous recording of signals from both electrode pairs.

All recorded signals were filtered to a passband of 0.5 to $30\,\mathrm{Hz}$ in with Fourier filter Matlab function which is presented as Appendix. Prior to analysis, all signals and their PSDs were visually examined to confirm that no abnormal peaks were present. A part containing only the noise floor was extracted from the signals, so obvious artifacts had minimal effect on the calculations. The minimum length of any extracted part was 2000 samples which corresponds to 20 seconds in time domain. The RMS values V_n of recorded signals were defined as standard deviations σ which corresponds to equation 2.8 when the mean value is $\mu = 0$. Due to AC coupling of the EEG recording system and later filtering with Matlab, the assumption of zero mean value is well justified. The previously defined internal RMS noise V_i of the measurement system was subtracted from the calculated RMS noises, resulting in electrode contact noise V_{ec}.

The measured impedances Z_{20} and the defined electrode contact RMS noise voltages V_{ec} were plotted as data points into a (Z_{20}, V_{ec}) graph. Theoretical thermal noise voltages V_{th} were calculated for the range of $\Delta R = 0$–$10\,\mathrm{M\Omega}$. The calculations were made according to equation 2.11, assuming room temperature $T = 293\,\mathrm{K}$ and the same passband Δf as mentioned above. The $V_{th}(R)$ curve was plotted in the same graph as the (Z_{20}, V_{ec}) data pairs. The PSDs were computed using a 256-sample window function.

Adding to that, a univariate analysis of variance was performed on the 10-based logarithms of Z_{20} and V_{ec} in order to assess the sources of variance of the experiment result data. The analysis was performed with Minitab statistics package (Minitab Inc., State College, PA, U.S.A.). The analysis included partitioning of the total sum of squares into components, an F-test, effect size estimation, and a power analysis.

3.3 Electrode contact stabilization

The stabilization of the electrode contact as a function of time was assessed by measuring Z_{20} values for 15 minutes after attaching electrodes to skin. The measurements were performed on forearm, and Elefix was used as gel. Both electrode sites were prepared with different amounts of skin abrasion prior to electrode attachment. The sites were abraded with 5, 10, 15, and 20 strikes of fine sandpaper. This was followed by attachment of electrodes. Z_{20} value was measured with $30\,\mathrm{s}$ intervals.

3.4 Susceptibility to motion artifacts

3.4.1 Repeatability and reproducibility of different motion artifact setups

In order to study the motion artifacts, a setup which reproduces the electrode motion as similarly as possible in all situations is needed. Adding to that, the motion artifact magnitudes are expected to vary between different individuals, as the skin properties between individuals vary. Thus, studying motion artifacts magnitudes is difficult.

Initially the reproducibility and repeatability of three different motion artifact setups were studied. Used setups were horizontal motion, vertical motion and vertical pressure. Horizontal and vertical motions were produced with a microservomechanism which moved the electrode either horizontally or vertically. The microservomechanism had a torque of $1.5\,\mathrm{kg\,cm^{-1}}$ with a $4.8\,\mathrm{V}$ supply voltage. It was used in a wiper-mode, meaning that the arms were moving back and forth with a fixed amount of rotation. The electrode ring spacer was connected to one end of the servo arm with a thick iron wire. The microservomechanism was fixed on a bench wise. Vertical pressure was produced by placing a cylindrically shaped object on top of the electrode.

A total of ten test subjects were used, with three repeated motions per subject with each setup. Signals were recorded with NeurOne EEG system because the GE EEG system has a more limited input range which can lead to amplifier saturation with a large enough artifact. If the amplifier saturates, the artifact magnitude can not be detected. All measurements were made on forearm with Elefix gel. Skin preparation prior to recording varied. Signals were recorded with ground and reference electrodes placed at a minimum distance of $10\,\mathrm{cm}$ from the electrode to which the motion was induced.

Prior to analysis, the recorded signals were low-pass filtered with a $30\,\mathrm{Hz}$ cut-off frequency. Motion artifacts were quantified as peak-to-peak fluctuations within a $5\,\mathrm{s}$ time window from the moment the motion was induced to the electrode. The whole peak-to-peak fluctuation is a relevant parameter because biopotential amplifiers have a limited input range. Each peak-to-peak value x_i was converted to ratio r_i to the sample median m within each setup according to equation

$$r_i = 1 - \frac{m(x_1, x_2, \ldots, x_n) - x_i}{m(x_1, x_2, \ldots, x_n)} \tag{3.2}$$

where $x_1, x_2, \ldots, x_n$ are all recorded values produced with a single setup. A two-way analysis of variance and gauge repeatability and reproducibility study were performed on r values recorded with different test subjects and motion artifact setups. The analyses were performed with Minitab statistics package (Minitab Inc., State College, PA, U.S.A.). The results are presented in Table 3.1 and 3.2. In Table 3.1 MS denotes mean square (sum of squares divided by degrees of freedom). In Table 3.2, VC is the variance component caused by each source and σ is the standard deviation of each source.

The mean values standard deviations of r_i within each setup were also calculated to assess reproducibility. The repeatability within subjects was further assessed by comparing the difference of maximum and minimum values to the median for each subject according to equation

$$s_i = \frac{\max(r_1, r_2, r_3) - \min(r_1, r_2, r_3)}{m(r_1, r_2, r_3)} \tag{3.3}$$

where r_1, r_2 and r_3 are three repeated artifacts for a single subject with the same setup.

Table 3.1. *Two-way analysis of variance with interaction analysis of motion artifact setups.*

Source	MS
Setup	$1.32 \cdot 10^{-4}$
Subject	$2.16 \cdot 10^{-5}$
Subject-Setup	$2.95 \cdot 10^{-5}$

Table 3.2. *Gage R&R analysis results of motion artifact setups.*

Source	VC	σ
Total Gage R&R	$1.03 \cdot 10^{-5}$	$3.21 \cdot 10^{-3}$
Repeatability	$7.41 \cdot 10^{-7}$	$8.61 \cdot 10^{-4}$
Reproducibility	$9.58 \cdot 10^{-6}$	$3.09 \cdot 10^{-3}$

Mean value and standard deviation of s_i were also calculated within each setup. Mean values and standard deviations for both r_i and s_i are presented in Table 3.3.

The mean square value for motion artifact setups is significantly larger than for subjects which means that the setups are a greater source of variance. The subject-setup interaction is not significant source of variation compared to setup. As a conclusion, even though the motion artifact magnitudes are likely to vary with different subjects, the used setups were significantly greater source of variance in this experiment.

The gage R&R study results show that the variance originating from reproducibility to total study variance is significantly greater than variance originating from repeatability. The standard deviations of reproducibility is also significantly larger than that of repeatability.

In order for the setup to have a good reproducibility, the standard deviation of r_i should be small compared to the mean. For vertical motion, the mean value and standard deviation are equal. The corresponding results of vertical pressure is not that good either as the standard deviation is significantly large compared to mean. Horizontal motion, instead, has the best result of these all, as the standard devitation is considerable smaller than mean.

The s_i values are already normalized, so only the mean is relevant. The mean of horizontal motion is the smallest, so this setup fared the best considering repeatability too. Thus, horizontal motion was selected as the setup to be used in further experiments.

Table 3.3. *Mean value and standard deviation r_i and s_i (Equations 3.2 and 3.3).*

Setup	$\mu(r_i)$	$\sigma(r_i)$	$\mu(s_i)$	$\sigma(s_i)$
Horizontal motion	1.15	0.42	0.27	0.20
Vertical motion	1.82	1.82	0.85	1.32
Vertical pressure	1.49	1.28	0.85	0.56

3.4.2 Horizontal motion artifact

Based on the earlier results, the horizontal motion was selected to be used. It was also decided to collect more contact noise data during these experiments. For the sake of contact noise measurement reproducibility, the measurements were performed with GE EEG system. None of the motion artifact magnitudes caused by horizontal motion from the previous experiment exceeded the input range of the GE EEG system, so the choice was feasible in that sense too. Measurements were made with a total of 11 subjects, with the electrodes placed on forearm. Elefix was used as gel.

The actual experiment protocol was as follows. First the ground and reference electrode sites were prepared by abrading semi-roughly with a fine sandpaper. Three sites for recording electrodes were placed on skin with varied skin preparation. Z_{20} was measured between each recording electrode paired with the reference electrode. One of the recording electrodes at a time was used to record contact noise signal for 30 seconds, after which a motion was induced to the electrode. The horizontal motion setup is presented in Fig. 3.2. The RMS contact noise voltage was computed as described earlier, and the motion artifact was quantified as a peak-to-peak voltage fluctuation of the signal within a 5 second time window from the moment the motion was induced. In a couple of occasions the electrode attachment was so poor that the electrode was disengaged due to the motion. These data points were excluded from the results.

With the used electrode configuration it is very improbable that the electrode can move with respect to skin as it is attached to it with a combination of an adhesive and a ring spacer. As a result, the examined motion artifacts are expected to originate mostly from stretching of skin, which causes variation in voltage E_{se} described earlier in Figure 2.4. Furthermore, as the gel is quite well encapsulated by the electrode with this configuration, it will follow possible movements of the electrode. Thus, the gel is not likely to move with respect to skin or electrode. As also mentioned earlier, with recessed electrodes the metal-electrolyte interface is not expected to be a major source of motion artifact [3].

3.5 Estimation of acceptable noise level

The operation of the seizure detection algorithm was studied with increasing noise added to EEG signals. Two recorded signals from patients receiving critical care were used. The signals were collected at London Health Sciences Centre, Ontario, Canada. The first signal was a control signal which contained no epileptic seizure activity. The other signal was an example of a clear detection of an epileptic seizure, and annotations of start and end points of the seizure were provided by Dr. G. Bryan Young, an expert neurologist.

A noise signal was created to simulate electrode contact noise by creating white noise and filtering it to certain frequency bands, and amplifying the bands with different coefficients and summing the amplified bands together. The created noise signal was summed

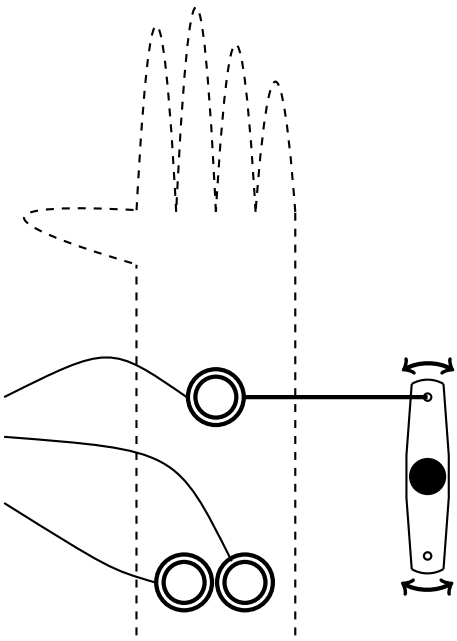

Figure 3.2. *An illustration of the used motion artifact setup. A sensing electrode placed on inner forearm is connected to a servomechanism arm which rotates back-and-forth around its centre axis (the black circle). The dimensions of the illustration are not exact. The distance from the moved electrode to reference and ground electrodes is 10 cm at minimum.*

to raw EEG signals at different magnitudes. The noisy raw EEG data was then processed with the algorithm, and the algorithm output variable describing evolution of seizures was assessed in order to find out how it behaved with the signals with different amounts of added noise.

The Matlab code used to generate contact noise signal is presented in Fig. 3.3. The code utilizes a Fourier filter which is presented as an appendix. The code inputs are signal sampling frequency, desired white noise standard deviation, and number of samples, that it the length of the noise signal. For each generated noise signal, the sampling frequency and signal length inputs are taken from the raw EEG signal to which the noise was summed. The code outputs are the created noise signal as a vector, and its RMS value calculated with *std* function.

In the code, the first step is to generate white noise with a set standard deviation and signal length with *randn* function. The total RMS value of the noise signal is based on the standard deviation, so it varied. The next step of the code is filtering the white noise to desired bands. The first band is from DC to 1 Hz, with a 3 Hz slope width between passband and stopband. The second band is from DC to 2 Hz, with a slope width of $f_s/2 - 2$ Hz. The third band is from 4 to 6 Hz with zero slope width at either cut-off frequency. Then the frequency bands are amplified with coefficients of 15, 1.2 and 0.5, respectively, and summed together. After summation the signal is low-pass filtered with a $f_s/2$ cut-off frequency with zero slope width. Total RMS values of added noise signals and their noise densities are presented in Table 3.4.

```
function output = contactnoise(fs,stdev,nsamples);
% create noise signal simulating electrode contact noise
% inputs: sampling frequency, white noise standard deviation (in
% volts), number of samples
% output struct: simulated noise signal and its RMS value (in volts)

% generate white noise column vector
noise = stdev.*randn(1,nsamples)';

% define frequency band limits in Hz
f1=1; f2=2; f4=4; f6=6;

% filter white noise to defined frequency bands
a1 = fflt(noise, fs, f1, 3, 'low'); %0-1 Hz
a2 = fflt(noise, fs, f2, fs/2-f2, 'low'); %0-2 Hz
a3 = fflt(noise, fs, f4, 0, 'high'); %4-6 Hz
a3 = fflt(a3, fs, f6, 0, 'low');

% amplify and sum filtered white noise
sum = 15*a1 + 1.2*a2 + 0.5*a3;

% low-pass filtering at fs/2 and finalizing output struct
output.signal = fflt(sum, fs, fs/2, 0, 'low');
output.rms = std(output.signal);

end
```

Figure 3.3. *Matlab code used to simulate contact noise signal.*

The abovementioned frequency bands and amplification coefficients were selected experimentally. Different values were tried and PSD of the resulting signal was visually evaluated. With the abovementioned values the resulting PSD resembles roughly PSDs of those contact noise signals which were computed from actually recorded signals. The used method is very simple and simplifies the contact noise signal quite a bit. However, based on the similarities of the PSDs, it can be used as a rough estimate of a realistic contact noise signal.

Fig. 3.4 presents a PSD curve of an example of a simulated contact noise signal. In this example the input parameters were a sampling frequency of $250\,\text{Hz}$, white noise mean of $1\,\mu\text{V}$, and signal length of 10000 samples. This signal has an RMS value of $2.1\,\mu\text{V}$ at the DC to $125\,\text{Hz}$ bandwidth.

The total noise level can not be precisely estimated with this method, because the noise level originally present in the raw EEG is not known. However, as the uncorrelated noise sources are summed together quadratically, the greater the added noise is compared to

Table 3.4. *Added noise RMS values at* 125 Hz *bandwidth and corresponding noise densities.*

RMS noise [µV]	Noise density [µV $Hz^{-1/2}$]
4.4	0.4
8.8	0.8
13.2	1.2
17.4	1.6
21.8	2.0
26.0	2.3
30.9	2.8
35.3	3.2
39.6	3.6
43.8	3.9

original noise, the more it will dominate the total noise. Thus, if the raw EEG is assumed to be relatively noise-free, the added noise can be used as a rough estimate of the total noise level.

The algorithm output variable, denoted EVO-OUT, was assessed based on its numerical values and the evolution of the curve as a function of time. EVO-OUT is based on the activity of all used EEG channel derivations. It has a scale from 0 to 100. A high value indicates seizure activity. If the signal is corrupted with noise and artefacts to such extent that the algorithm cannot interpret it, EVO-OUT will be zero. The principles of the algorihtm are described in detail by Tanner [5]. A rough guideline is that if its value exceeds 8.0, the algorithm indicates seizure activity to be present. The control signal was used to evaluate whether false positive seizure detections occur due to added noise. EVO-OUT curves of all signals after adding noise were visually evaluated, and their maximum values were noted. A false positive was found, and the point at which it occurred was examined in detail by examining one channel derivation of EEG signals with some of the different amounts of added noise at that time point. The channel derivation selection was based on assessing other algorithm output variables which indicated that this particular channel had the most significant effect on EVO-OUT value at that time point.

In the clear detection signal there were two peaks at the EVO-OUT curve during the seizure. The second peak is an indication of post-ictal suppression, and if its value decreases significantly, post-ictal suppression is not detected by the algorithm as a rough guideline. Furthermore, a significant reduction of the first peak value also indicates that added noise affects the algorithm operation. EVO-OUT curves with different amount of added noise during the seizure were visually evaluated. One EEG channel derivation was selected and the signal during the seizure was evaluated with some different amounts of added noise. The used channel was selected because other algorithm variables indicated that particular channel to have the most significant effect on EVO-OUT during post-ictal suppression. EVO-OUT curves for the same noisy signals were plotted. [49]

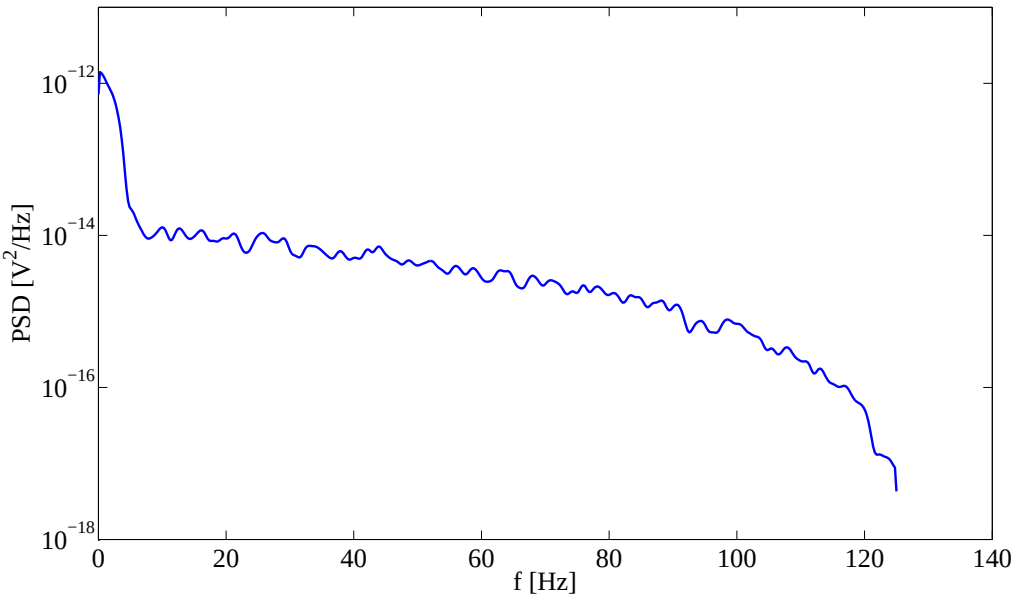

Figure 3.4. *An example of a simulated electrode contact noise signal presented in frequency domain.*

4. RESULTS

4.1 Electrode contact impedance and noise

4.1.1 Descriptive results

The metal-electrolyte noise of two electrodes face-to-face in Abralyt 2000 and Elefix gels were $V_{me} = 70\,\text{nV}$ and $V_{me} = 92\,\text{nV}$, respectively. As the amplifier internal noise was $87\,\text{nV}$, this means that with Abralyt the metal-electrolyte noise cannot be distinguished from amplifier noise. With Elefix, however, the corresponding result is slightly above amplifier internal noise at all frequencies. There is a considerable peak near DC. PSDs of the internal noise signal and signals recorded electrodes face-to-face in both gels are presented in Fig. 4.1. With Abralyt 2000, the contact impedance was $Z_{20} = 103\,\Omega$, while with Elefix it was $Z_{20} = 88\,\Omega$.

Results of the measured electrode contact impedances and electrode contact noise measured with Abralyt 2000 gel on earlobe and forearm are presented in Fig. 4.2 and Fig. 4.3, respectively. In both of the figures a relationship between contact impedance and noise exists. The measured electrode contact noise is generally significantly larger than expected thermal noise.

The contact impedance and noise results with Elefix gel are presented in Fig. 4.4 and Fig. 4.5, respectively. Also these figures indicate a relationship. Measured contact noise is generally significantly larger than expected thermal noise in these cases too.

PSDs of two signals measured from earlobe with different gels are presented in Figs 4.6. Electrode contact impedance had a value of $Z_{20} \simeq 18\,\text{k}\Omega$ for both of the signals. The noise is significantly larger with Elefix than with Abralyt 2000 through the whole examined freqency band.

PSDs of five signals recorded from one subject on earlobe with Abralyt 2000 are presented in Fig. 4.7. Z_{20} was $1.150\,\text{M}\Omega$ for the first signal, and due to skin preparation it was gradually reduced all the way to $5\,\text{k}\Omega$ of the last signal. The corresponding V_{ec} values for the signals were $6.16\,\mu\text{V}$, $1.17\,\mu\text{V}$, $1.08\,\mu\text{V}$, $0.884\,\mu\text{V}$, and $0.552\,\mu\text{V}$, respectively. With all contact impedance magnitudes, most of the contact noise appears at very low frequencies. No skin preparation was done prior to recording of the first curve. When comparing the first curve to the rest it can be seen that the PSD curves have a steeper decline starting at around $1\,\text{Hz}$ due to skin preparation.

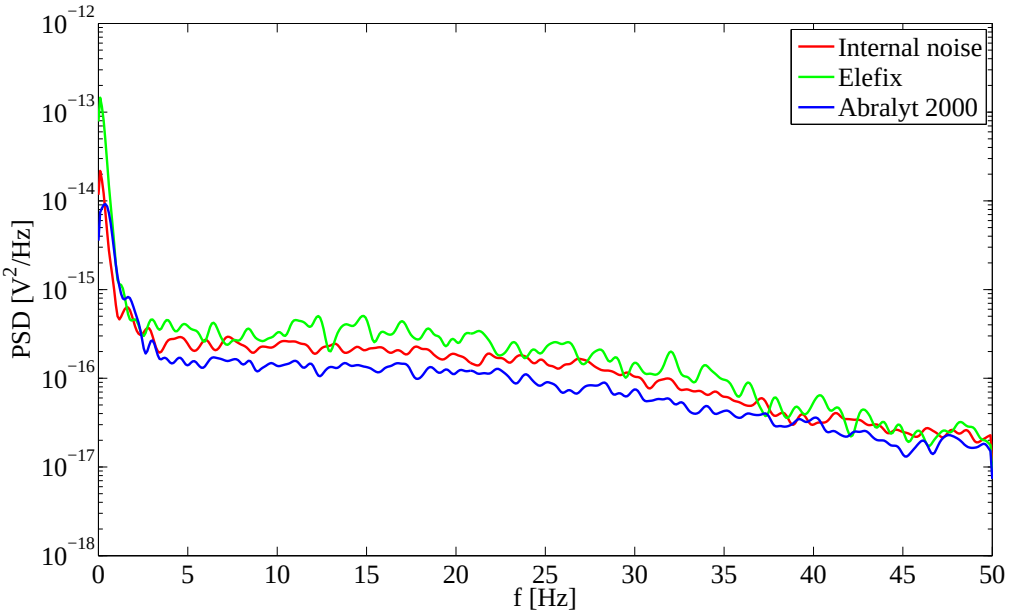

Figure 4.1. *PSDs of amplifier internal noise, and noise recorded with electrodes face-to-face with both gels.*

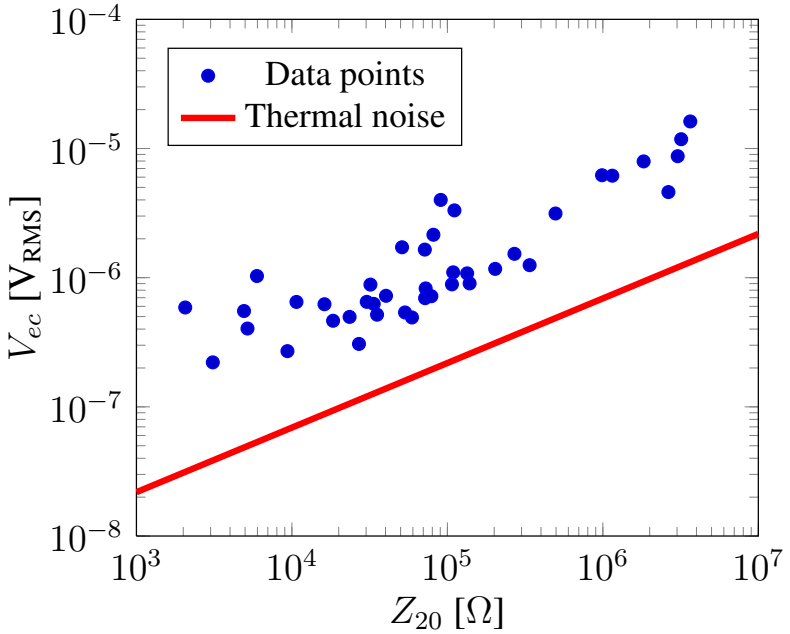

Figure 4.2. *Contact impedance and noise from earlobe with Abralyt2000;* $\Delta f = 0.5$–$30\,\mathrm{Hz}$.

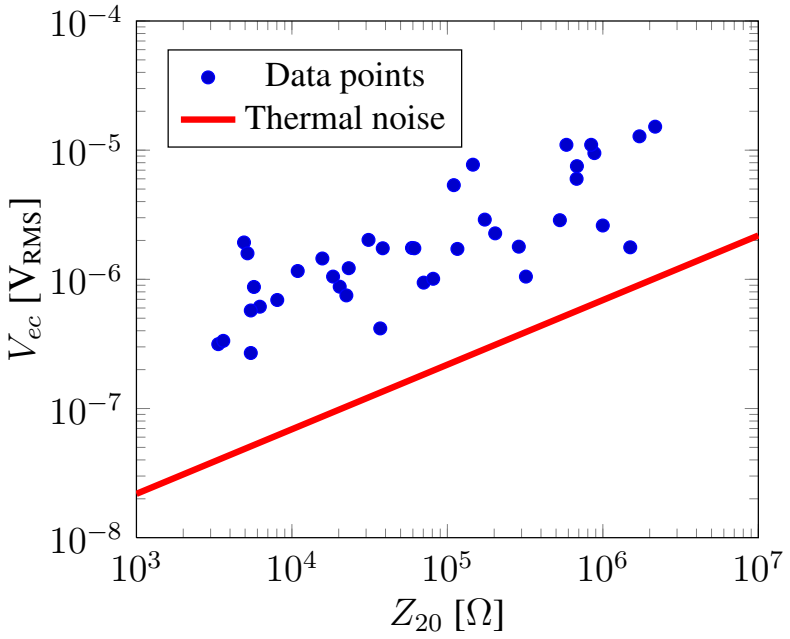

Figure 4.3. *Contact impedance and noise from foream with Abralyt2000;* $\Delta f = 0.5$–30 Hz.

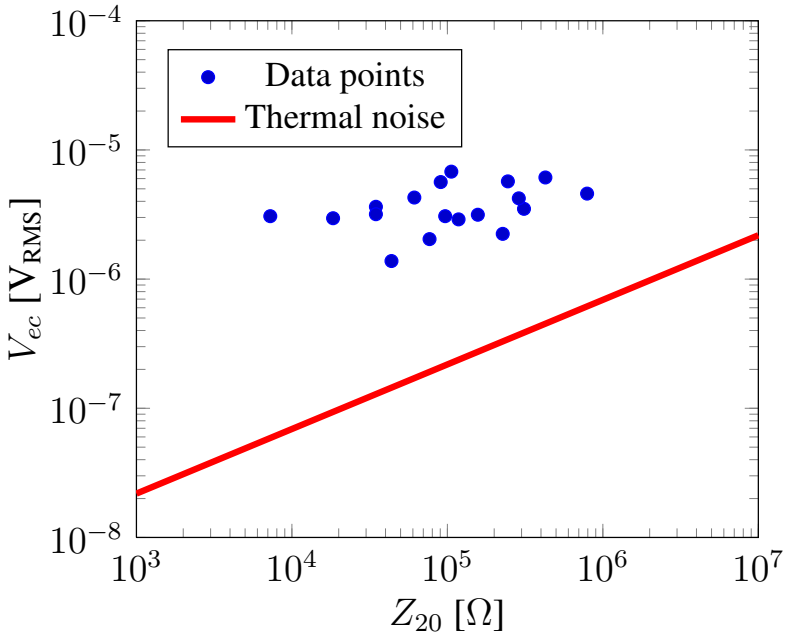

Figure 4.4. *Contact impedance and noise from earlobe with Elefix;* $\Delta f = 0.5$–30 Hz.

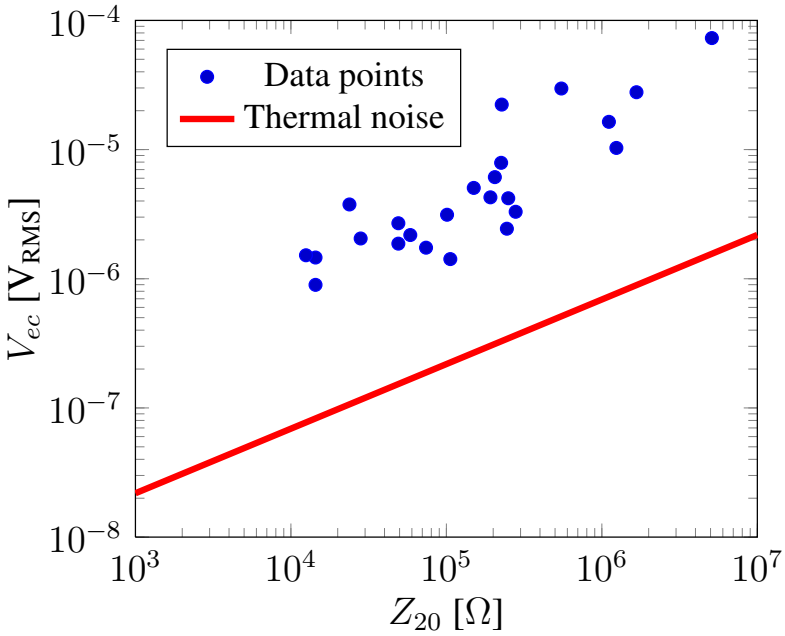

Figure 4.5. *Contact impedance and noise from forearm with Elefix;* $\Delta f = 0.5$–$30\,\mathrm{Hz}$.

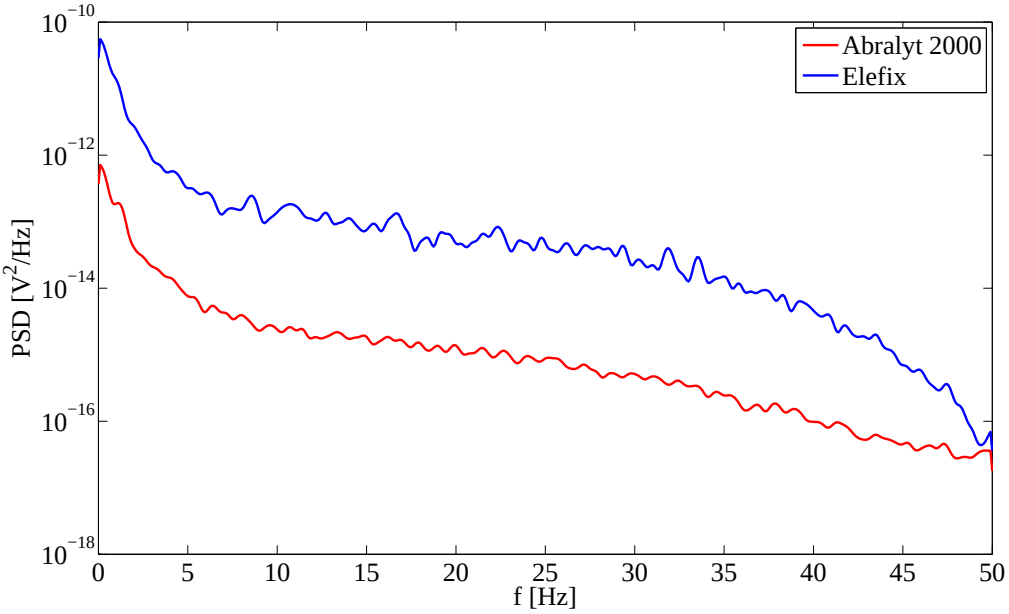

Figure 4.6. *PSDs of two signals measured from earlobe with Abralyt 2000 and Elefix with same* $Z_{20} \simeq 18\,\mathrm{k\Omega}$ *for both signals.*

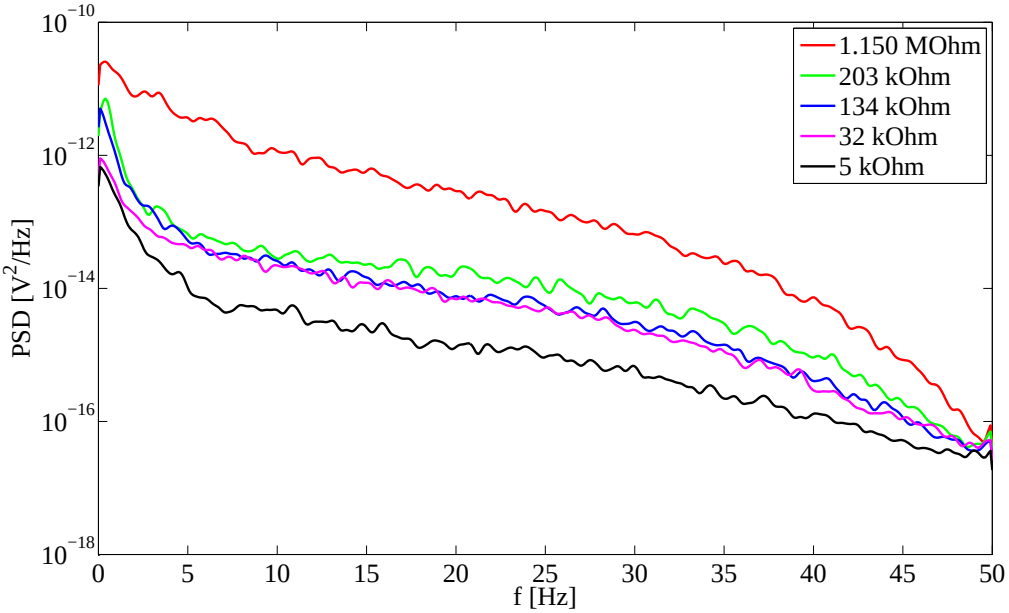

Figure 4.7. *PSDs of five signals recorded from one subject on earlobe with Abralyt 2000 with different Z_{20} values.*

4.1.2 Statistical analysis

The results of the unvariate analysis of variance are presented in Table 4.1, MS is the mean square value (sum of squares per degrees of freedom) of each variance source and σ is the data dispersion. From the results it is clear that Z_{20} is the greatest source of variation. Used gel has a more significant effect than body location.

Table 4.1. *Univariate analysis of variance of* $\log_{10}(V_{ec})$.

Source	MS	σ
$\log_{10}(Z_{20})$	15.824	0.000
Location	0.461	0.010
Gel	3.176	0.000
Loc+Gel	0.181	0.106

4.2 Electrode contact stabilization

Results of electrode contact stabilization experiments with different amounts of skin abrasion with sandpaper prior to electrode attachment are presented in Fig. 4.8. All curves are quite similarly shaped.

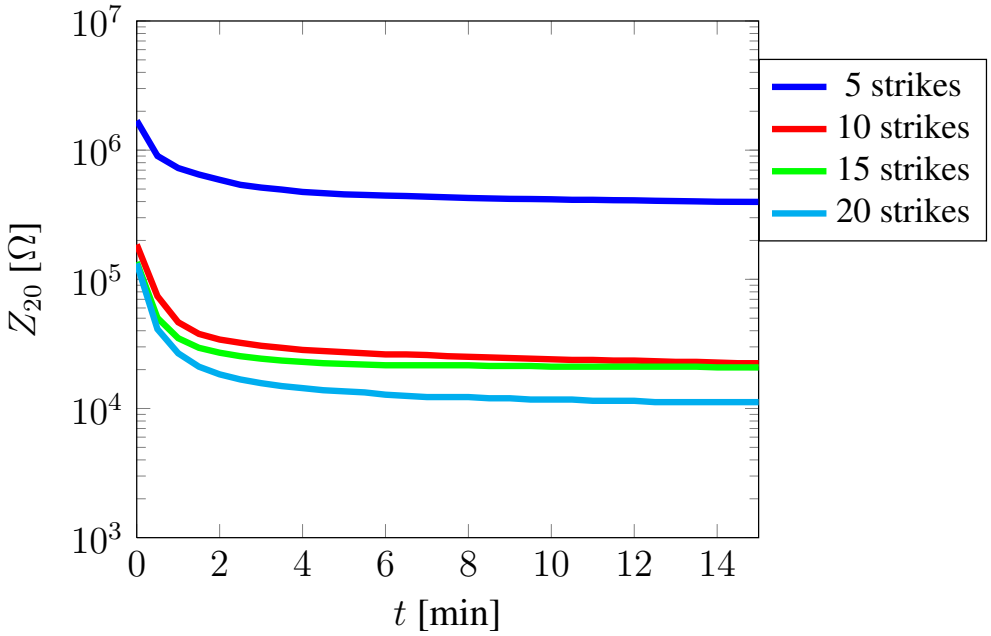

Figure 4.8. *Electrode contact stabilization time based on* Z_{20} *value with different amounts of skin preparation.*

4.3 Susceptibility to motion artifacts

The results of the horizontal motion artifact experiments are presented in Figure 4.9. The results indicate that a relationship between contact impedance and motion artifact magnitude exists, as a decrease Z_{20} values seems to decrease to motion artifact magnitude.

The results of additional electrode contact impedance and noise experiments measured on forearm are presented in Figure 4.10. Based on the figure, a relationship between contact impedance and contact noise exists in this case also.

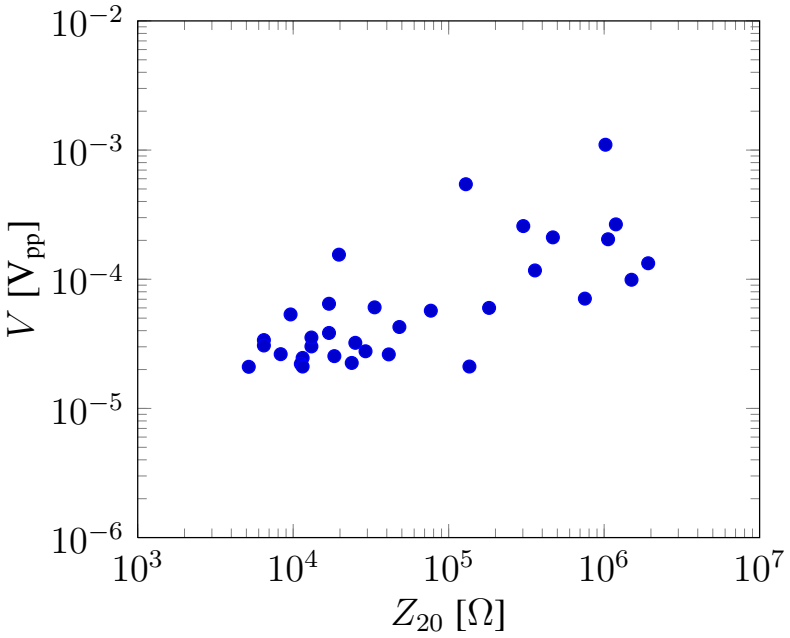

Figure 4.9. *Susceptibility to motion artifacts as a function of contact impedance;* Δf *=0.5–30* Hz

4.4 Estimation of acceptable noise level

The maximum EVO-OUT values for the control signal with different amounts of added noise are presented in Fig. 4.11. The initial value with no added noise is 5.3. With the smallest amount of added noise the maximum value is 10.6, which exceeds the limit given for an indication of seizure activity. As this was the control signal, this is a false positive detection. After more noise is added, the maximum values have the tendency to decrease below the seizure indication limit.

The EVO-OUT curves of added noise levels 0, 4.35 and 17.4 µV around the time point where the false positive detection occurred are presented in Fig. 4.12. The curve is plotted for a 42 s time window. It must be noted that the maximum values presented in Table 4.11 did not always occur during the same time window, which is why the curves of 4.12 and values of Table 4.11 do not correspond. The EVO-OUT curves of noise levels 0 and 4.4 µV differ in the peak value and the decrease rate after the peak. The EVO-OUT curve for noise level 17.4 µV is below 0.5 during this time window.

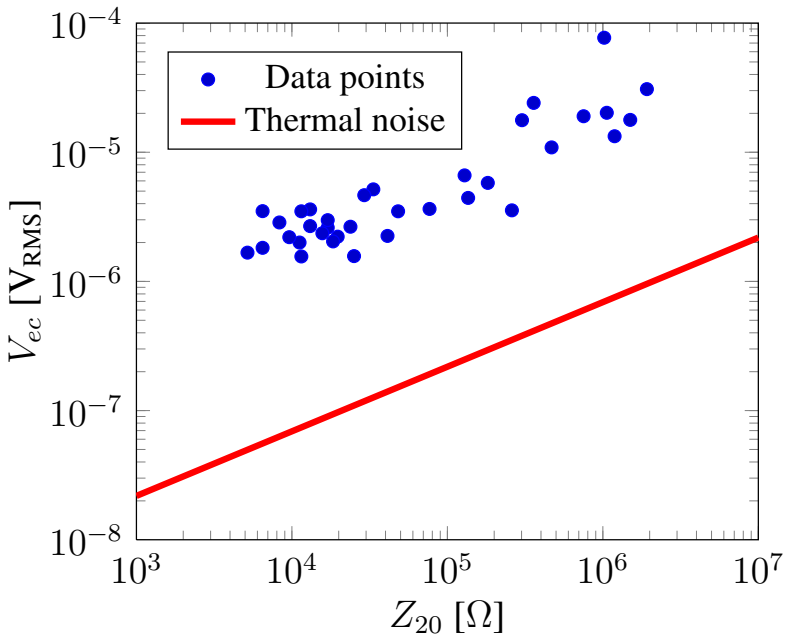

Figure 4.10. *Additional data of contact impedance and noise from forearm with Elefix;* Δf = 0.5–30 Hz.

EEG tracings for F3-C3 channel derivation during the same time window with the same added noise levels are presented in Figs. 4.13, 4.14 and 4.15. In the first two signals there are only slight differences due to the added noise. However, the third signal is already significantly altered due to added noise.

Fig. 4.16 presents the EVO-OUT curves during the clear seizure detection (a 70 s time window) with no added noise and five different amounts of added noise. The start and end points of the seizure are noted with dashed vertical lines. It can be seen that the value of the second peak starts to decrease significantly immediately with the smallest amount of added noise, and it keeps decreasing as more noise is added. The value of the first peak does not start to decrease so drastically. Only at added noise level 21.8 µV there is a significant decrease.

EEG tracings for T3-P4 channel derivation during the same time window with the some of the added noise levels are presented in Figs. 4.17, 4.18, 4.19 and 4.20. In the first two signals, the main difference seems to be at post-ictal suppression, as with the noisy signal the amplitudes are clearly higher. The third and fourth signal are significantly distorted due to added noise.

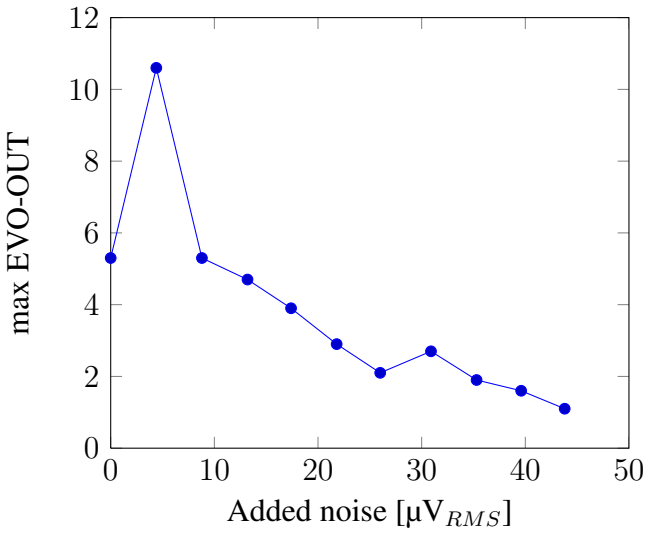

Figure 4.11. *Maximum EVO-OUT values of control signals as a function of added noise.*

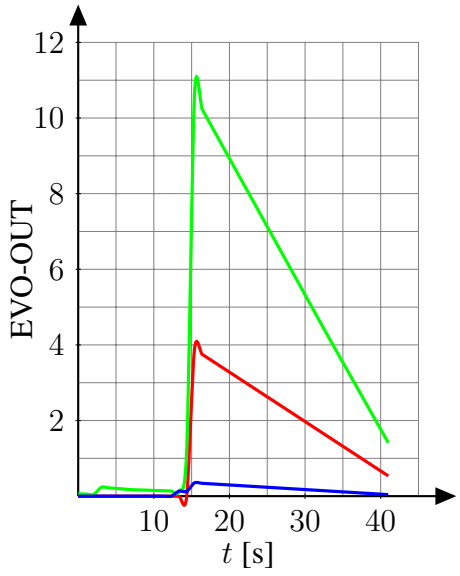

Figure 4.12. *EVO-OUT values during false positive seizure detection for control signal: red, green and blue denote added noise levels 0, 4.4 and 17.4* μV*, respectively.*

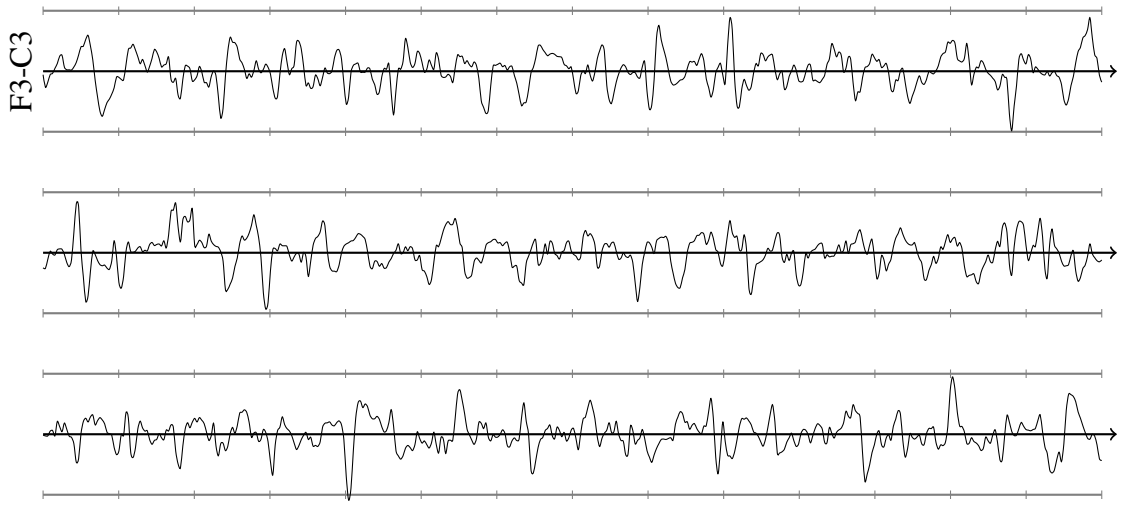

Figure 4.13. *EEG tracing of control signal with no added noise. The tick marks on the horizontal axes indicate one second intervals, and the gray lines on top and bottom of the baseline level indicate* $\pm 50\,\mu\mathrm{V}$ *amplitude levels.*

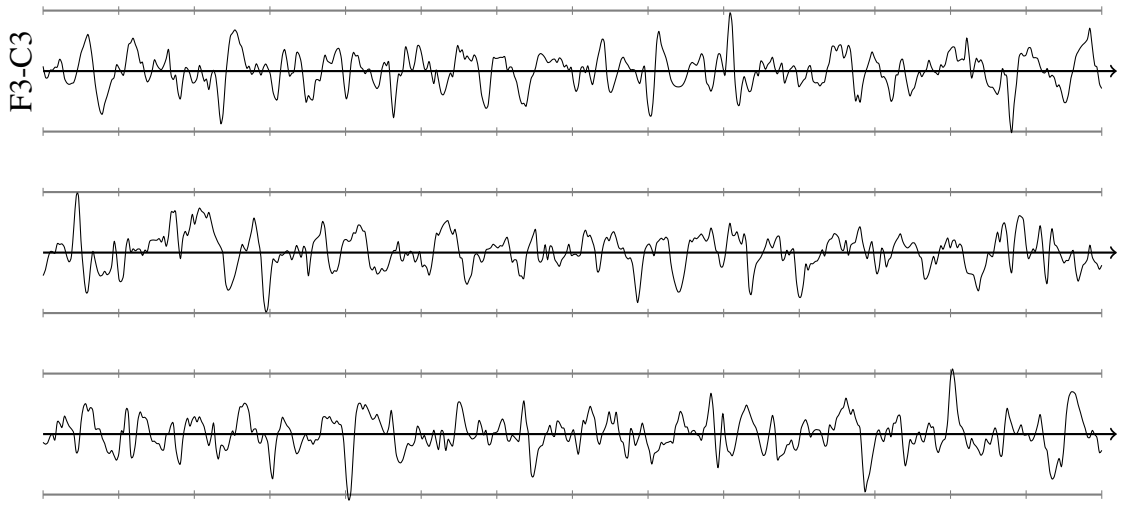

Figure 4.14. *EEG tracing of control signal with* $4.4\,\mu\mathrm{V}$ *added noise; the false positive occurred during this tracing. The tick marks on the horizontal axes indicate one second intervals, and the gray lines on top and bottom of the baseline level indicate* $\pm 50\,\mu\mathrm{V}$ *amplitude levels.*

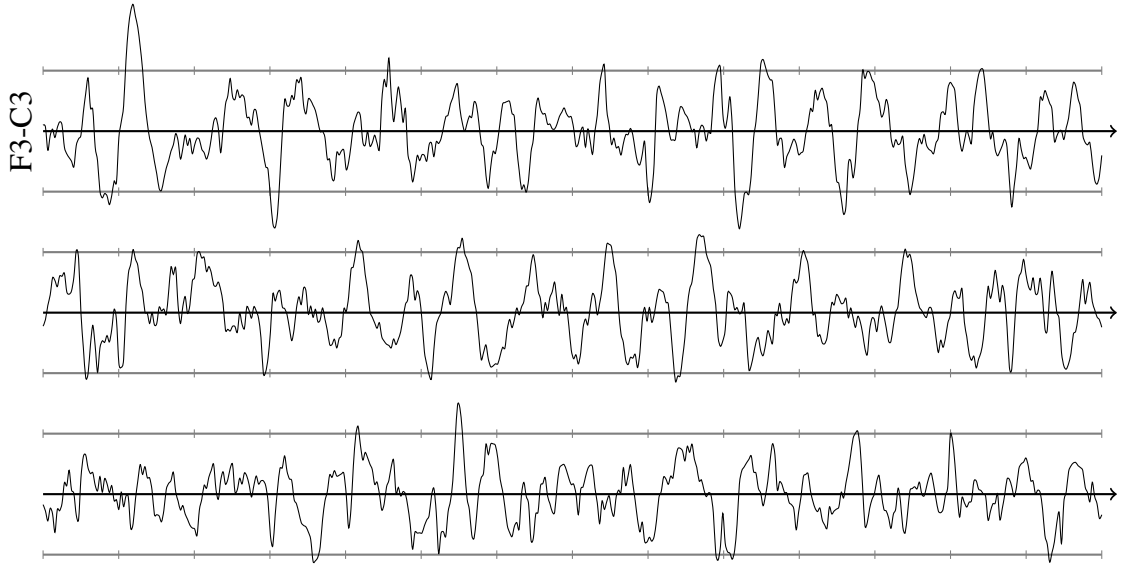

Figure 4.15. *EEG tracing of control signal with* $17.4\,\mu V$ *added noise. The tick marks on the horizontal axes indicate one second intervals, and the gray lines on top and bottom of the baseline level indicate* $\pm 50\,\mu V$ *amplitude levels.*

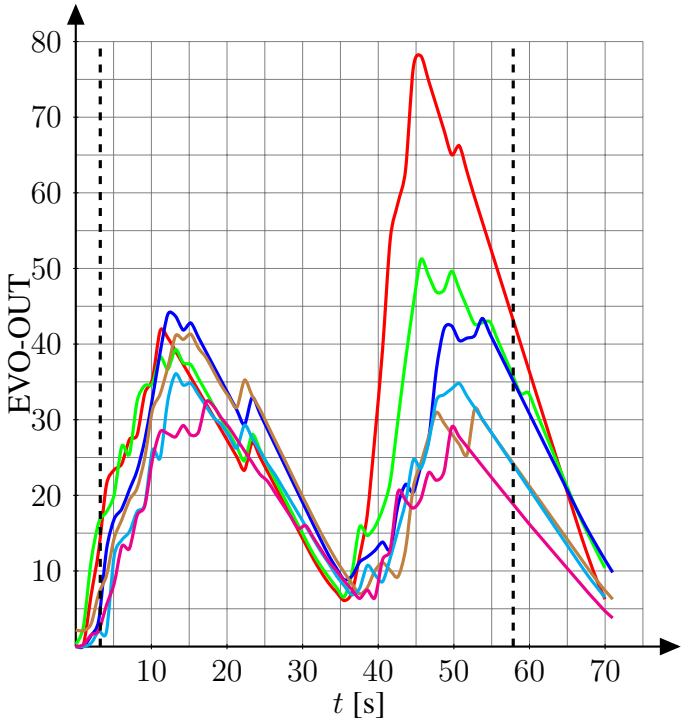

Figure 4.16. *EVO-OUT curves during clear seizure detection; red, green, blue, brown, cyan and magenta denote 0, 4.4,, 8.8, 13.2, 17.4 and* $21.8\,\mu V$ *of added noise, respectively. Dashed lines indicate start and end points of the seizure.*

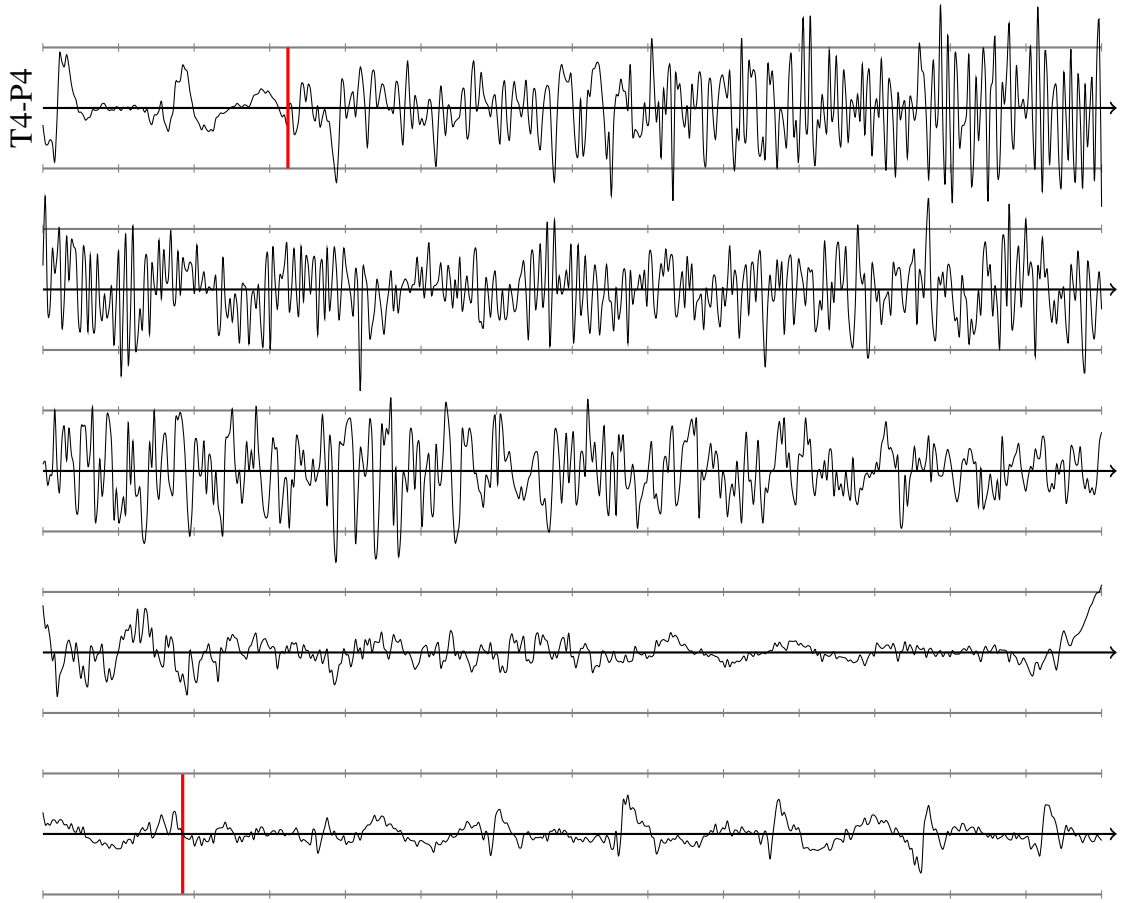

Figure 4.17. *EEG tracing during clear seizure detection with no added noise. The red lines indicate start and end points of the seizure. The tick marks on the horizontal axes indicate one second intervals, and the gray lines on top and bottom of the baseline level indicate* $\pm 50\,\mu\mathrm{V}$ *amplitude levels.*

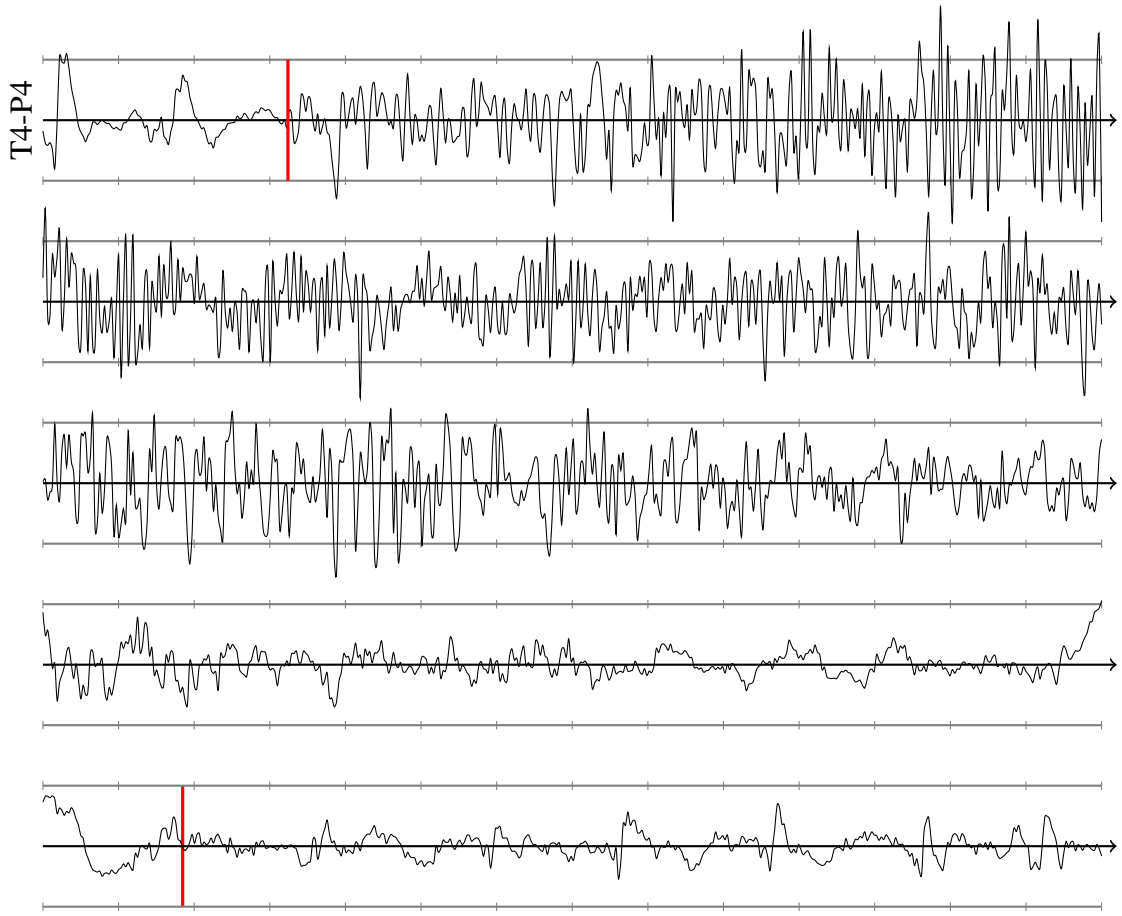

Figure 4.18. *EEG tracing during clear seizure detection with* $4.4\,\mu V$ *added noise l. The red lines indicate start and end points of the seizure. The tick marks on the horizontal axes indicate one second intervals, and the gray lines on top and bottom of the baseline level indicate* $\pm 50\,\mu V$ *amplitude levels.*

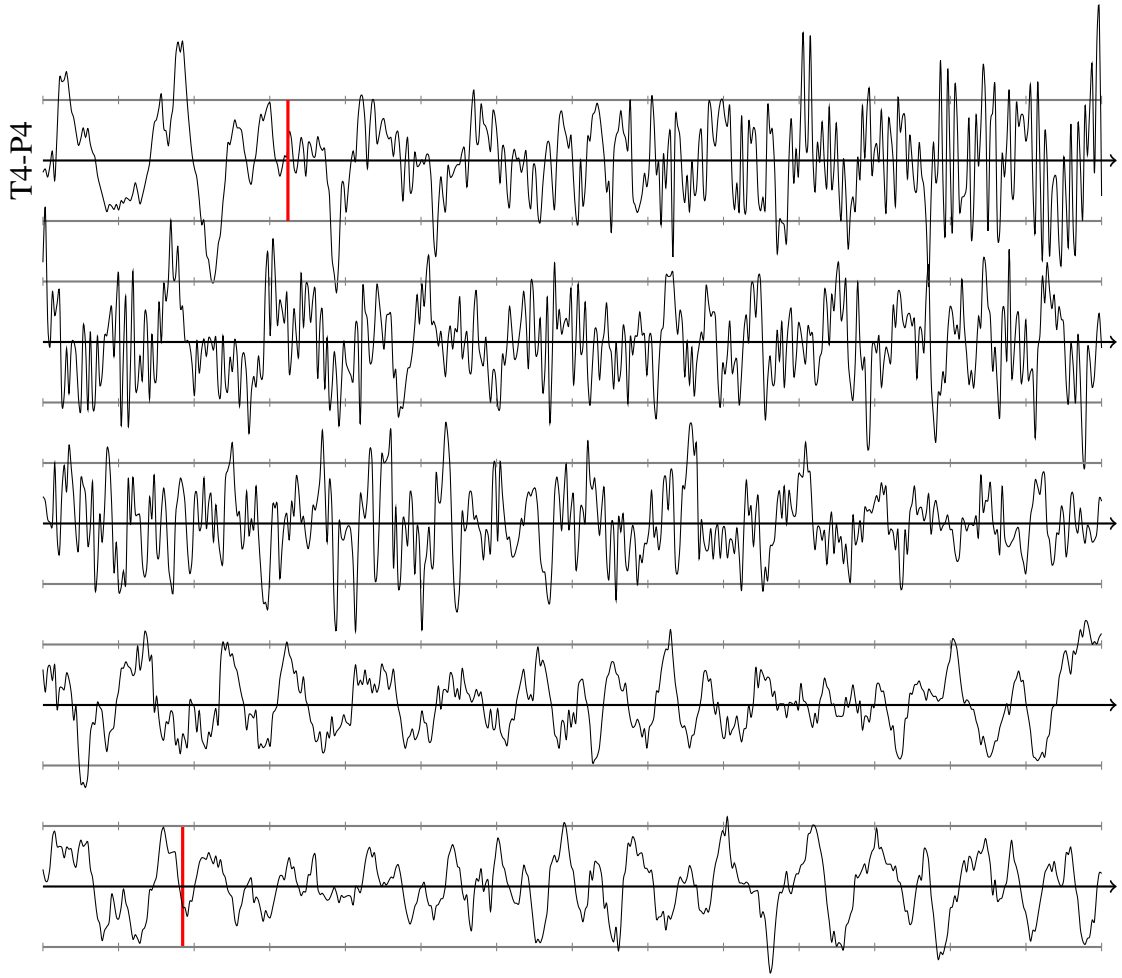

Figure 4.19. *EEG tracing during clear seizure detection with* $17.4\,\mu V$ *added noise. The red lines indicate start and end points of the seizure. The tick marks on the horizontal axes indicate one second intervals, and the gray lines on top and bottom of the baseline level indicate* $\pm 50\,\mu V$ *amplitude levels.*

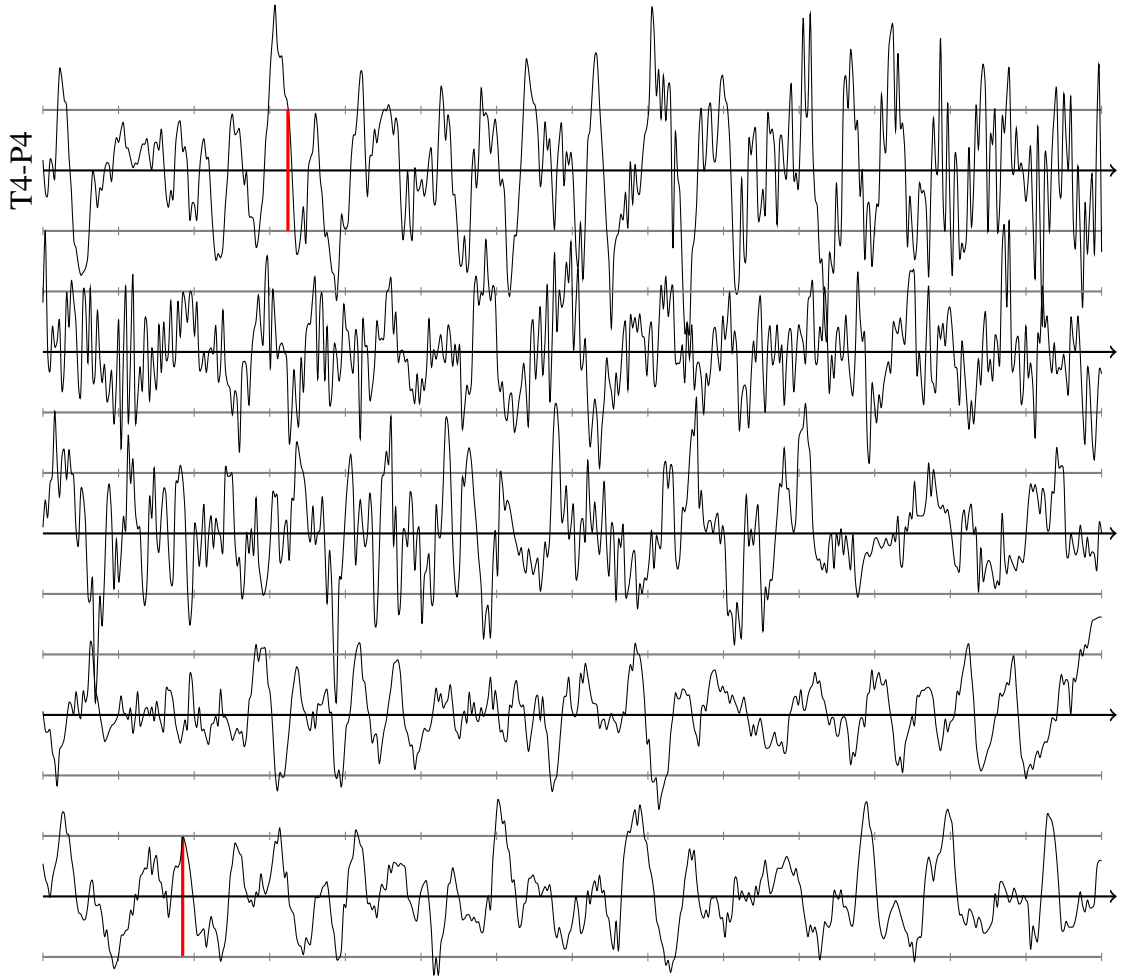

Figure 4.20. *EEG tracing during clear seizure detection with* $21.8\,\mu V$ *added noise. The red lines indicate start and end points of the seizure. The tick marks on the horizontal axes indicate one second intervals, and the gray lines on top and bottom of the baseline level indicate* $\pm 50\,\mu V$ *amplitude levels.*

5. DISCUSSION

5.1 Electrode contact impedance and noise

Based on the article by Horikawa et al., it was an expected result that the metal-electrolyte noise of $70\,\mathrm{nV}$ of Abralyt 2000 cannot be distinguished from amplifier noise ($87\,\mathrm{nV}$) [31]. Even though the metal-electrolyte noise of $92\,\mathrm{nV}$ of Elefix is slighty above amplifier noise, is it still a negligibly small factor considering total electrode contact noise. The PSD curves of metal-electrolyte noise with both gels are similarly shaped compared to amplifier noise, except that with Elefix the PSD curve has a considerable peak near DC.

Even though the metal-electrolyte impedance was smaller with Elefix than with Abralyt 2000, slighty more noise was generated with Elefix. This supports the theory that noise mechanisms other than thermal noise also contribute to metal-electrolyte noise, as their effects can not totally be estimated based on impedance.

Based on measurements made on both earlobe and forearm with Abralyt 2000, it can be concluded that a relationship between electrode contact impedance and electrode-skin noise exists as expected. The measured electrode contact noise is generally significantly larger than expected thermal noise which is also an expected result. It is also evident that there is variation of V_{ec} values at approximately the same Z_{20} values. This is expected as differences of individual test subjects are expected to be a significant source of variation.

When the results from earlobe and forearm are compared, it can be seen that the variation of data points is significantly larger on measurements made on forearm. The first explanation could be the more probable presence of muscle activity at forearm than at earlobe. Consequently, in some of the data points muscle activity was likely to corrupt the signal.

Based on the corresponding measurements made with Elefix, a relationship between contact impedance and noise also seems to exist. In these cases there does not seem to be much greater variation in data points measured on forearm compared to those measured on earlobe. It is evident that both data sets with Elefix contain too few data points at low Z_{20} values which are of a great interest in the context of this thesis.

According to the results, it seems that with Elefix gel the electrode contact noise is larger than with Abralyt 2000. This is supported by the results of metal-electrolyte noise measurements, where Elefix caused more noise even though it had a smaller Z_{20} value, although the differences are of an insignicant magnitude considering total electrode contact properties. This might be due to different chemical compositions of the two gels,

which could result in differences of noise generated in the electrochemical processes. As mentioned earlier, Abralyt 2000 should support the characteristic of sintered electrodes in order to produce a good-quality signal. This could explain why there is a clear difference in noise magnitudes. However, with other types of electrodes this might not be the case.

Another difference with the gels is their mechanical properties. Abralyt 2000 is quite fluent, while Elefix is clearly more viscous. Thus, Abralyt 2000 is more likely to fill inhomogeneities on skin surface better which leads to an increased contact area. An increased contact area naturally leads to a decreased contact impedance, but it is possible that it will affect contact noise through some other mechanism as well.

The increased contact noise caused by Elefix is further supported by Fig. 4.6. Even though Z_{20} was same for both signals, there was clearly more noise present in the signal recorded with Elefix. The PSDs have essentially the same shape. Only the baseline differs between them, so the gel seems to affect the contact noise at all examined frequencies. V_{ec} had values of $0.464\,\mu V$ and $2.96\,\mu V$ for the two examined signals, respectively. However, as only two signals are examined, it is likely that individual properties of the test subject have an effect on the result too. In fact, it is possible that the approximate difference of curves of slightly less than 20 dB throughout the frequency spectrum can originate mostly from the test subjects.

From the two data sets measured from forearm, the variation of data points was smaller with Elefix. As Elefix seems to generate more noise, it could be that the additional noise masks the signals where muscle activity is minimal, and therefore those signals cannot be distinguished from the signals where muscle activity is evident. As we do not understand the mechanisms of how all noise sources are summed at the electrode-skin interface, this possibility cannot be proved and thus remains open.

The voltage noise densities from the experiments in this study are between 0.0403 and $2.9577\,\mu V\,Hz^{-1/2}$ for earlobe, and 0.0491 and $13.3279\,\mu V\,Hz^{-1/2}$ for forearm. Table 5.1 presents the noise densities and RMS noises calculated from the results of Huigen et al. and Fernández and Pallás-Areny compared with the results of this study [2,30].

The minimal values correspond well with those from the previously reported articles. The maximum value of the experiments of this study is much higher than those values from the previous articles, but seems logical as Z_{20} in that particular measurement was about $5\,M\Omega$, as seen in Fig. 4.5. Fernández and Pallás-Areny used pre-gelled Ag-AgCl electrodes (3M Company, St. Paul, MN, U.S.A.) which enable a fairly low contact impedance even without skin preparation. A likely result that in their experiments the contact impedances were always significantly lower than the highest of those in the experiments of this study. This would also give reason for the higher noise values of the experiments of this study. However, no data on impedances is presented by Fernández and Pallás-Areny, so further comparison is not possible. Huigen et al. measured the contact impedance at DC, so comparison is not possible in that case either. The impedance

Table 5.1. *Comparison of contact noise results from forearm with previous studies. RMS value defined for* Δf = 0.5–30 Hz.

Reported result	Noise density [μV Hz$^{-1/2}$] Min	Max	RMS [μV] Min	Max
This study	0.0491	13.3279	0.2690	72.9570
Huigen et al. [2]	0.0447	0.2236	0.2248	1.2247
Fernández and Pallás-Areny [30]	0.0447	0.6708	0.2448	3.6741

values in their experiments were between 2 and 600 kΩ.

There were big differences between initial Z_{20} values of different test subjects on both electrode locations and with both gels. This supports the theory of variation of skin properties between individuals. However, there might also be some other issues between individuals affecting the results, such as a thorough cleansing or rubbing of skin on the day before the experiments. Also the reduction of Z_{20} as a result of skin preparation seems to be quite different between individuals in all of the experiments even though the preparation method was kept as similar as possible during each experiment. This also supports the same theory.

The group of test subjects consisted of both male and female colleagues of the author. The ages of the subjects were between 20 to 50 years. However, all subjects were fair-skinned which limits the generalization of the results to a larger population.

Some test subjects got visible marks on their forearm as a result of the experiments done with Abralyt 2000 gel. Such marks did not occur with Elefix. The explanation could be the different skin preparation methods, as only the small area the size of a cotton swab was prepared when using Abralyt 2000, while with Elefix the area was always larger. The recuperation period of the marks lasted up to 10 days in the worst case. It can be concluded that if the desired contact impedance level is very low, damage to skin is likely to occur. Based on verbal feedback of some test subjects, Elefix seems to cause more irritation. This is expected as Abralyt 2000 does not contain chloride ions.

During the contact impedance measurement, the maximal current density in the circuit was 0.013 mA cm^{-2} based on the fed voltage and bias resistor value. At such low current densities, the metal-electrolyte interface impedance is not expected to be dependent on current density [13]. Impedances were measured quite briefly after electrode attachment, and signals were recorded after that, so no fixed time was given for the electrode contact to stabilize. As discussed in further in this thesis, Z_{20} decreases very rapidly initially. The electrode cables were attached to the impedance circuit only after the gel insertion, so it is likely that the steepest decrease was avoided. However, it is still likely, that during signal recording Z_{20} decreased from its initial value. V_{ec} is also expected to decrease with time. These both add to the uncertainty of the measurement.

The statistical analysis showed the contact impedance to be the greatest source of vari-

ation on electrode contact noise. This is an expected result as a relationship between the them was expected to exist. The gel was found to cause more variation than body location. This supports the earlier dicussed results seen in the (Z_{20}, V_{ec}) graphs. The result means that it would be useful to take the effect of the gel into account if compromises between signal quality and contact impedance must be made.

When the relationship of Z_{20} and V_{ec} is analyzed, it must be taken into account that with these results Z_{20} is the total impedance of two electrode contacts. EEG recording devices measure the individual contact impedances for each electrode. Thus, if the impedances values of both a sensing and a reference electrode are balanced, a Z_{20} value of say $20\,\mathrm{k}\Omega$ of these results would correspond to $10\,\mathrm{k}\Omega$ for both individual electrodes.

5.2 Electrode contact stabilization

All curves representing electrode contact impedance as a function of time with different amount of skin preparation show quite a similar shape. Initially Z_{20} decreases quite rapidly. However, after about one minute the decrease rate becomes much smaller. After ten minutes the rate is practically negligible in all of the curves.

There is practically a difference of one decade of inital Z_{20} values between the curve with the lightest preparation and the other curves. The final Z_{20} values of the curves also show same kind of behavior. There is little difference between final Z_{20} values of the curves with 10 and 15 strikes of preparation, while the final Z_{20} values of the curve with the strongest preparation is approximately half of that of the two previous curves. Based on this result, it seems that 20 abrasive strikes with a fine sandpaper will result in a Z_{20} value of about $10\,\mathrm{k}\Omega$, which means about $5\,\mathrm{k}\Omega$ per individual electrodes.

5.3 Horizontal motion artifact

A decreasing contact impedace, meaning an increased skin preparation, was found to decrease magnitudes of motion artifacts. Thus the results support those of Tam and Webster [3]. At low Z_{20} values the artifact magnitudes are fairly well concentrated in the range of 20–60 µV, with a slight tendency to increase with increasing Z_{20} value. As Z_{20} increases, the variation in artifact magnitudes seems to increase as well. This is expected based on earlier results of de Talhouet and Webster [4].

The motion artifact setup is an evident uncertainty factor in these experiments, as confirmed in the analysis of different setups. Adding to that, the differences in skin properties between individuals are also a source of variance. As the magnitude of motion artifacts is at least an order of magnitude larger than the contact noise, the used gel should only have a very small effect on motion artifact magnitudes. However, it is possible that the gel modulates the deformations of skin caused by mechanical movement, and thus with different gels the motion artifacts might have slightly different magnitudes.

As described earlier, with the used electrode configuration the motion artifact is likely to originate mainly from variations of skin voltage. Thus, these results can be generalized only to similar electrode configurations where recessed electrodes are attached to the patient with an adhesive. Adding to that, the used horizontal movement limits the generalization of the results as well. In a realistic situation, vertical electrode movement can be just as or even more likely to occur than horizontal, depending on the exact situation of course. With a headset implemented with fabric straps, even a combination of both horizontal and vertical electrode movement is very much possible to occur.

The results of additional contact noise measurements made during motion artifact experiments are consistent with the previous results. They provide more data on the low impedance range which was missing from the earlier experiments. From the data it can be concluded that with Z_{20} range of 5–$20\,\mathrm{k\Omega}$ the contact noise seems to settle at around 1–$5\,\mu\mathrm{V}$ at the examined bandwidth in quite a consistent manner.

5.4 Estimation of acceptable noise level

With the control signal, the algorithm output maximum value increased initially as noise was added. After the initial increase the maximum value started to decrease. A false positive seizure detection occurred with the smallest amount of added noise. This was an unexpected result, as the examined EEG signal did not differ much between the no-noise signal and the signal with the smallest amount of added noise. However, after more noise was added, maximum algorithm output variables started decreasing as expected. The third plotted EEG tracing was already significantly distorted.

There was a clear effect on the algorithm behavior due to the smallest amount of added noise with the clear detection signal. The second peak of the output variable decreased significantly, meaning that the added noise had an effect on the detection of post-ictal suppression. The effect of the noise on post-ictal suppression can be seen from the EEG tracings of the no-noise signal and the signal with the smallest amount of added noise, as with the latter the amplitudes are larger during post-ictal suppression. As more noise was added, the second peak on the output variable decresed more. However, the first peak started to decrease significantly only after a quite a lot of noise was added to the signal. The third and fourth plotted EEG tracings were significantly altered due to noise, but the algorithm output still had fairly high values.

Based on these experiments, it is possible that with noisy signals the algorithm will have false positive seizure detections. On clear detections, increased noise seems to have the most effect on detection of post-ictal suppression. In conclusion, even a relatively small amount of added noise was found to alter the algorithm behavior significantly. The small amount in this case was $4.4\,\mu\mathrm{V}$ at a $125\,\mathrm{Hz}$ bandwidth, which corresponds to a noise density of $0.4\,\mu\mathrm{V\,Hz^{-1/2}}$. At a $30\,\mathrm{Hz}$ bandwidth this would correspond to an RMS noise of about $2.2\,\mu\mathrm{V}$. This value corresponds to a maximum contact impedance of approximately

20 kΩ in Fig. 4.10 which presented data measured with Elefix on forearm. Due to the limited amount of data measured from earlobe with Elefix, that noise level cannot be related to that data. However, as mentioned earlier, the noise level originally present in the used signals is not known, so this is only a very rough approximation. As even this small amount of added noise altered the algorithm behavior, it is suggested that for the correct algorithm operation the noise level should be relatively low.

Considering the second output variable peak during the seizure, the sensitivity of the output variable dropped to about half of that of the output value with no added noise somewhere between noise levels 8.8 and 13.2 µV. If assumed that the point is 11 µV, which corresponds to a noise density of 1.0 µV $\text{Hz}^{-1/2}$. Within the 30 Hz bandwidth, that would correspond to an RMS value of 5.4 µV. Again this would correspond to a maximum contact impedance of about 30 kΩ when looking at Fig. 4.10.

In order to assess the issue in a more consistent way, actual EEG data should be collected with individual electrode contact impedance levels such as 10 to 20 kΩ at 20 Hz, and the algorithm behaviour should be assessed. It would also be useful to have similar EEG signals with different amount of noise shown to neurologists, who could estimate at which level the signal quality is no more acceptable. As an experienced neurologist will always detect seizures better than any algorithm, this method would rule out signal quality levels at which it is no more possible to detect seizures reliably.

5.5 Reliability of the results

In the contact impedance and noise experiments, the stabilization of the electrode contact is a clear factor contributing to measurement uncertainty, as no fixed time was given for the contact to stabilize. Another factor is the used sintered Ag-AgCl electrodes, as with another electrode type the results might be slightly different. In the motion artifact experiments, the setup causing the motion artifact was likely to contribute to measurement uncertainty significantly, as the motions were not likely exactly similar in all cases. The used electrode configuration and the utilization of only horizontal movement both limit the generalization of the results. The group of test subjects were all fair-skinned which also limits the generalization of the results of both sets of experiments.

Previously, only Huigen et al. have assessed the relationship of electrode contact impenance and noise in a similar way as in this thesis [2]. They too found a relationship between the two quantities, although their sample size was significantly smaller than the sample size in this study. Adding to that, they measured the impedance at DC, so the results cannot be compared directly.

The previous results by de Talhouet and Webster on the relationship of electrode contact impedance and motion artifact magnitude had similar characteristics than the results of this thesis [4]. However, their sample size was rather limited, as was the one in this thesis. Morever, they measured the impedance at different frequency, and their setup for

production of electrode motions was different.

With the algorithm behavior study, there are clear uncertainty factors. First of all, only two signals were used. In order to fully assess the algorithm performance, is significantly larger signal database is needed. Secondly, the algorithm is still under development, and thus with future version the results might be different. Moreover, the created contact noise signal is a very rough estimate of a realistic contact noise signal.

5.6 Implications of the results to biopotential amplifier design

As mentioned earlier, important biopotential amplifier characteristics considering the work in this thesis are input impedance and input dynamic range. Input impedance can be divided to common-mode and differential input impedances. The larger the common mode input impedance is, the less effect common-mode voltage has on the recording. Differential input impedance should also be high, as no loading of the electrode-skin signal source is desired. It was found that with contact impedances of less than $20\,\mathrm{k}\Omega$ the contact noise is likely to be within reasonable values. If the amplifier has no input line filters, contact impedance values of this range are not a problem, as with modern IAs the input impedances are in the range of gigaohms. However, if input line filters are utilized, the selection of resistance and capacitance values should be done with care. Maximizing the input impedance values also minimizes the effect of contact impedance mismatches and the change of contact impedances over time.

The input dynamic range should be high enough so that the amplifier will not saturate due to electrode offset voltages and signal artefacts. As discussed earlier, the motion artifacts produced in the experiments do not simulate possible motions in realistic situations very well. Thus, the numerical values of motion artifact magnitudes from the experiments can not be used as a guideline considering the input dynamic range. In conclusion, the motion artifact experiments done in this thesis do not provide useful information considering the amplifier design.

The noise properties of the amplifier should be of a high importance in this application. As electrode contact noise is potentially higher than in traditional EEG applications, the contribution of the amplifier to total noise should be minimal. Noise performance should be used as a criterion for selection of all integrated circuits. The amplifier bandwidth should be as narrow as possible to minimize noise.

5.7 Suggestions for future work

As the gel was found to contribute to electrode contact noise significantly, it would be useful to know more about the gel properties which might be the causes of this. It would also be interesting to broaden the study to contain more electrolytic gels. The effect of gels should also be assessed with other types of electrodes. In any possible further studies

of similar purpose, the contact impedances should be measured at the same frequency as in this study in order for the results to be comparable with those of this study.

6. CONCLUSION

This thesis aimed to evaluate how accurately biopotential signal quality can be estimated as a function of electrode contact impedance. Two factors contributing to signal quality were studied: total electrode contact noise and motion artifact magnitude. Electrodes were placed on skin and the contact impedance was measured, which was followed by signal recording. Two different body sites and two different electrolytic gels were used when contact noise was studied. Motion artifacts were studied on one body site with one electrolytic gel, and the electrode motion was produced be moving the electrode in horizontal direction with a microservomechanism. Finally, the behavior of a previously implemented algorithm for detection of epileptic seizures from EEG signal was studied by adding noise to two EEG signals: one with no epileptic seizure activity, and the other with a clear epileptic seizure. The added noise signal simulated a noise signal generated at the electrode contact.

It was found that electrode contact impedance can be used as a rough predictor of electrode contact noise. It was also found out that the electrolytic gel can have a significant impact on the amount of noise generated at the electrode contact. The used body site was found to have a smaller effect. The motion artifact magnitudes were found to decrease as electrode contact impedance decreased. The larger the contact impedance was, the larger were the variations of motion artifact magnitudes. The behavior of the seizure detection algorithm was found to be significantly altered even with a small amount of added noise.

REFERENCES

[1] E. McAdams, "Bioelectrodes," in *Encyclopedia of Medical Devices and Instrumentation* (J. G. Webster, ed.), vol. 1, Hoboken, U.S.A.: John Wiley & Sons, Inc., 2nd ed., 2006.

[2] E. Huigen, A. Peper, and C. A. Crimbergen, "Investigation into the origin of the noise of surface electrodes," *Medical & Biological Engineering & Computing*, vol. 40, pp. 332–338, 2002.

[3] H. W. Tam and J. G. Webster, "Minimizing Electrode Motion Artifact by Skin Abrasion," *IEEE Transactions on Biomedical Engineering*, vol. 24, pp. 134–139, 1977.

[4] H. de Talhouet and J. G. Webster, "The origin of skin-stretch-caused motion artifacts under electrodes," *Physiological Measurement*, vol. 17, pp. 81–93, 1996.

[5] A. Tanner, "Automatic seizure detection using a two-dimensional EEG feature space." M.Sc. thesis. Aalto University, School of Science, 2011.

[6] E. Ikonen, "EEG-sensor set — Long term use as a design challenge." Bachelor thesis. Aalto University, School of Art and Design, 2010.

[7] A. Savelainen, "Movement Artifact Detection from Electroencephalogram Utilizing Accelerometer." M.Sc. thesis. Aalto University of Science and Technology, 2011.

[8] J. D. Bronzino, "Principles of Electroencephalography," in *The Biomedical Engineering Handbook* (J. D. Bronzino, ed.), Boca Raton, U.S.A.: CRC Press LLC, 2nd ed., 2000.

[9] H. Jasper, "The ten-twenty electrode system of the International Federation," *Electroencephalography and Clinical Neurophysiology*, vol. 10, pp. 371–375, 1958.

[10] J. W. Clark Jr., "The Origin of Biopotentials," in *Medical Instrumentation: Application and Design* (J. G. Webster, ed.), New York, U.S.A.: John Wiley & Sons, Inc., 4th ed., 2009.

[11] J. Partanen, "Aivosähkötoiminnan fysiologiaa," in *Sähköiset aivomme* (H. Lang, V. Häkkinen, T. A. Larsen, J. Partanen, and U. Tolonen, eds.), Suomen kliinisen neurofysiologian yhdistys ry, 1994.

[12] M. R. Neuman, "Biopotential electrodes," in *Medical Instrumentation: Application and Design* (J. G. Webster, ed.), New York, U.S.A.: John Wiley & Sons, Inc., 4th ed., 2009.

[13] L. A. Geddes, *Electrodes and the Measurement of Bioelectric Events*. New York, U.S.A.: Wiley-Interscience, 1972.

[14] P. Ask, P. Å. Öberg, S. Ödman, T. Tenland, and M. Skogh, "EEG Electrodes. A Study of Electrical and Mechanical Long-term Properties," *Acta Anesthesiologica Scandinavica*, vol. 33, pp. 281–311, 1979.

[15] L. A. Geddes, "Historial evolution of circuit models for the electrode-electrolyte interface," *Annals of Biomedical Engineering*, vol. 25, pp. 1–14, 1997.

[16] J. Riistama, "Characterisation of wearable and implantable physiological measurement devices." D.Sc. thesis. Tampere University of Technology, 2010.

[17] S. Grimnes and Ø. G. Martinsen, *Bioimpedance & Bioelectricity Basics*. London, U.K.: Academic Press, 2000.

[18] A. M. Klingman, "Skin permeability: Dermatologic aspects of transdermal drug delivery," *American Heart Journal*, vol. 108, no. 1, pp. 200–207, 1984.

[19] Y. W. Chien, "Development of transdermal drug delivery systems," *Drug Development and Industrial Pharmacy*, vol. 13, no. 4 & 5, pp. 589–651, 1987.

[20] D. Bliss, "Anatomy: The Skin." National Cancer Institute. Available online: http://visualsonline.cancer.gov/details.cfm?imageid=4604, visited February 29, 2012.

[21] S. Rothman, *Physiology and Biochemistry of the Skin*. Chicago, U.S.A.: The University of Chicago Press, 1956.

[22] J. C. Lawler, M. J. Davis, and E. C. Griffith, "Electrical characteristics of the skin. The impedance of the surface sheath and deep tissues.," *Journal of Investigative Dermatology*, vol. 34, pp. 301–308, 1960.

[23] J. Rosell, J. Colominas, P. Riu, R. Pallás-Areny, and J. G. Webster, "Skin impedance from 1 Hz to 1 MHz," *IEEE Transactions on Biomedical Engineering*, vol. 35, pp. 649–651, 1988.

[24] J. J. Ackmann and M. Seitz, "Methods of complex impedance measurements in biological tissue," *CRC Critical Reviews in Biomedical Engineering*, vol. 11, no. 4, pp. 281–311, 1984.

[25] Ø. G. Martinsen, S. Grimnes, and E. Haug, "Measuring depth depends on frequency in electrical skin impedance measurements," *Skin Research and Technology*, vol. 5, pp. 179–181, 1999.

[26] P. Tallgren, "DC-stable electrode-skin interface for human EEG recordings," tech. rep., HUT Applied Electronics Laboratory series E5, 2005.

[27] T. C. Ferree, P. Luu, G. S. Russell, and D. M. Tucker, "Scalp electrode impedance, infection risk and EEG data quality," *Clinical Neurophysiology*, vol. 112, pp. 536–544, 2001.

[28] Centers for Disease Control, "Recommendations for Preventing Transmission of Human Immunodeficiency Virus and Hepatitis B Virus to Patients During Exposure-Prone Invasive Procedures." Available online: http://www.cdc.gov/mmwr/preview/mmwrhtml/00014845.htm, visited November 2, 2011.

[29] C. Gondran, E. Siebert, S. Yacoub, and E. Novakov, "Noise of surface bio-potential electrodes based on NASICON ceramic and Ag-AgCl," *Medical & Biological Engineering & Computing*, vol. 34, pp. 460–466, 1996.

[30] M. Fernández and R. Pallás-Areny, "Ag-AgCl Electrode Noise in High-Resolution ECG Measurements," *Biomedical Instrumentation & Technology*, vol. 34, pp. 125–130, 2000.

[31] M. Horikawa, H. Harada, and M. Yarita, "Detection Limit in Low-amplitude EEG Measurement," *Journal of Clinical Neurophysiology*, vol. 20, pp. 45–53, 2003.

[32] A. C. Metting van Rijn, A. Peper, and C. Grimbergen, "High-quality recording of bioelectric events. Part 1 Interference reduction, theory and practice," *Medical & Biological Engineering & Computing*, vol. 29, pp. 389–397, 1990.

[33] American Clinical Neurophysiology Society, "Guideline 1: Minimum Technical Requirements for Performing Clinical Electroencephalography," February 2006. Available online: http://www.acns.org/pdfs/Guideline%201.pdf, visited September 26, 2011.

[34] International Organisation of Societes for Electrophysiological Technology, "Guidelines for Digital EEG," April 1999. Available online: http://www.oset.org/img/guidelines/digitalEEG.pdf, visited September 26, 2011.

[35] J. L. Semmlow, *Biosignal and Biomedical Image Processing: MATLAB-Based Applications*. New York, U.S.A.: Marcel Dekker, Inc., 2004.

[36] S. Franco, *Design with Operational Amplifiers and Analog Integrated Circuits*. New York, U.S.A.: McGraw-Hill, 3rd ed., 2002.

[37] J. M. Clochesy, L. Cifani, and K. Howe, "Electrode site preparation techniques: A follow-up study," *Heart & Lung*, vol. 20, pp. 27–30, 1991.

[38] A. B. Simakov and J. G. Webster, "Motion Artifact from Electrodes and Cables," *Iranian Journal of Electrical and Computer Engineering*, no. 2, pp. 139–143, 2010.

[39] S. Ödman and P. Å. Öberg, "Movement-induced potential motion artifact by skin abrasion," *Medical & Biological Engineering & Computing*, vol. 16, pp. 159–166, 1982.

[40] D. C. Smith and J. R. Wace, "Surface electrodes for physiological measurement and stimulation," *European Journal of Anaesthesiology*, vol. 12, pp. 451–469, 1995.

[41] J. G. Webster, "Reducing motion artifacts and interference in biopotential recording," *IEEE Transactions on Biomedical Engineering*, vol. 31, pp. 823–826, 1984.

[42] K. J. Hayes, "Wave analyses of tissue noise and muscle action potentials," *Journal of Applied Physiology*, vol. 15, pp. 749–752, 1960.

[43] J. C. Huhta and J. G. Webster, "60-Hz Interference in Electrocardiography," *IEEE Transactions on Biomedical Engineering*, vol. BME-20, no. 2, pp. 91–101, 1973.

[44] M. R. Neuman, "Biopotential Amplifiers," in *Medical Instrumentation: Application and Design* (J. G. Webster, ed.), New York, U.S.A.: John Wiley & Sons, Inc., 4th ed., 2009.

[45] Analog Devices, Inc., "AD620 datasheet, rev. H." Available online: http://www.analog.com/static/imported-files/data_sheets/AD620.pdf, visited September 28, 2011.

[46] A. C. Metting van Rijn, A. Peper, and C. Grimbergen, "High-quality recording of bioelectric events. Part 2 Low-noise, low-power multichannel amplifier design," *Medical & Biological Engineering & Computing*, vol. 29, pp. 433–440, 1991.

[47] EASYCAP GmbH, "EASY CAP — Product List." Available online: http://www.easycap.de/easycap/e/products/products.htm, visited August 23, 2011.

[48] J. Virtanen, "Drying of electrode gels." Unpublished, 2010.

[49] A. Tanner, 2012. Personal communication.

A. APPENDIX — FOURIER FILTER

This Matlab code was originally written by Juha Virtanen. Some comments were added by Ilkka Hokajärvi.

```
function m=fflt(m, fs, cornerfrq, slopefrq, ftype)
% FFLT Fourier filter
% parameters: matrix, sampling frequency, corner frequency (Hz),
% slope width (Hz), type ('high', 'low', 'notch')

tscale = (1/fs)*size(m,1);
fsamp = 1/tscale;
mask = zeros(size(m,1),1);

% generate filter vector for low-pass filter
if strcmp(ftype, 'low'),
    hedge = round((cornerfrq + slopefrq ) / fsamp);
    ledge = round(cornerfrq / fsamp);
    %fill with ones, passband
    mask(1:ledge) = 1;
    mask(size(m,1) - ledge:size(m,1)) = 1;
    %lp slope
    if slopefrq > 0,
    step = 1 / (hedge - ledge);
    for i=1:hedge-ledge,
            mask(i+ledge) = 1-(i*step);
            mask(i+(size(m,1)-hedge)) = (i*step);
        end;
    end;
end

% generate filter vector for high-pass filter
if strcmp(ftype, 'high'),
    ledge = round((cornerfrq - slopefrq ) / fsamp);
    hedge = round(cornerfrq / fsamp);
```

```
    %fill with ones, passband
    mask(hedge:size(m,1)-hedge) = 1;
    %lp slope
    if slopefrq > 0,
    step = 1 / (hedge - ledge);
    for i=1:hedge-ledge,
            mask(i+ledge) = (i*step);
            mask(i+(size(m,1)-hedge)) = 1 - (i*step);
        end;
    end;
end

% generate filter vector for notch filter
if strcmp(ftype, 'notch'),
    mask = ones(size(m,1),1);
    notchlow = round((cornerfrq - (slopefrq/2))/fsamp);
    notchhigh = round((cornerfrq + (slopefrq/2))/fsamp);
    mask(notchlow:notchhigh) = 0;
    mask(size(m,1) - notchhigh : size(m,1) - notchlow) = 0;
end

% replicate filter vector to matrix with desired amount of columns
tmp = mask;
for i=1:size(m,2),
   mask(:,i) = tmp;
end

% perform DFT for input matrix
for i=1:size(m,2),
   m(:,i) = fft(m(:,i));
end

% multiply with filter matrix
m = m .* mask;

% perform inverse DFT
for i=1:size(m,2),
   m(:,i) = real(ifft(m(:,i)));
end
```

```
end
```